GUARD: A Safe Reinforcement Learning Benchmark

Anonymous authors
Paper under double-blind review

Abstract

Due to the trial-and-error nature, it is typically challenging to apply RL algorithms to safety-critical real-world applications, such as autonomous driving, human-robot interaction, robot manipulation, etc, where such errors are not tolerable. Recently, safe RL (*i.e.*, constrained RL) has emerged rapidly in the literature, in which the agents explore the environment while satisfying constraints. Due to the diversity of algorithms and tasks, it remains difficult to compare existing safe RL algorithms. To fill that gap, we introduce GUARD, a **G**eneralized **U**nified S**A**fe **R**einforcement Learning **D**evelopment Benchmark. GUARD has several advantages compared to existing benchmarks. First, GUARD is a generalized benchmark with a wide variety of RL agents, tasks, and safety constraint specifications. Second, GUARD comprehensively covers state-of-the-art safe RL algorithms with self-contained implementations. Third, GUARD is highly customizable in tasks and algorithms. We present a comparison of state-of-the-art on-policy safe RL algorithms in various task settings using GUARD and establish baselines that future work can build on.

1 Introduction

Reinforcement learning (RL) has achieved tremendous success in many fields over the past decades. In RL tasks, the agent explores and interacts with the environment by trial and error, and improves its performance by maximizing the long-term reward signal. RL algorithms enable the development of intelligent agents that can achieve human-competitive performance in a wide variety of tasks, such as games (Mnih et al., 2013; Silver et al., 2018; OpenAI et al., 2019; Vinyals et al., 2019), manipulation (Popov et al., 2017; Chen et al., 2023; Agostinelli et al., 2019; Shek et al., 2022), autonomous driving (Isele et al., 2019; Kiran et al., 2022; Gu et al., 2022a), robotics (Kober et al., 2013; Brunke et al., 2022), and more. Despite their outstanding performance in maximizing rewards, recent works (Garcıa & Fernández, 2015; Gu et al., 2022b; Zhao et al., 2023) focus on the safety aspect of training and deploying RL algorithms due to the safety concern in real-world safety-critical applications, *e.g.*, human-robot interaction, autonomous driving, etc. As safe RL topics emerge in the literature, it is crucial to employ a standardized benchmark for comparing and evaluating the performance of various safe RL algorithms across different applications, ensuring a reliable transition from theory to practice. A benchmark includes 1) algorithms for comparison; 2) environments to evaluate algorithms; 3) a set of evaluation metrics, etc. There are benchmarks for unconfined RL and some safe RL, but not comprehensive enough (Duan et al., 2016; Brockman et al., 2016; Ellenberger, 2018–2019; Yu et al., 2019; Osband et al., 2020; Tunyasuvunakool et al., 2020; Dulac-Arnold et al., 2020; Zhang et al., 2022a).

To create a robust safe RL benchmark, we identify three essential pillars. Firstly, the benchmark must be **generalized**, accommodating diverse agents, tasks, and safety constraints. Real-world applications involve various agent types (e.g., drones, robot arms) with distinct complexities, such as different control degrees-of-freedom (DOF) and interaction modes (e.g., 2D planar or 3D spatial motion). The performance of algorithms is influenced by several factors, including variations in robots (such as observation and action space dimensions), tasks (interactive or non-interactive, 2D or 3D), and safety constraints (number, trespassibility, movability, and motion space). Therefore, providing a comprehensive environment to test the generalizability of safe RL algorithms is crucial.

Secondly, the benchmark should be **unified**, overcoming discrepancies in experiment setups prevalent in the emerging safe RL literature. A unified platform ensures consistent evaluation of different algorithms

in controlled environments, promoting reliable performance comparison. Lastly, the benchmark must be **extensible**, allowing researchers to integrate new algorithms and extend setups to address evolving challenges. Given the ongoing progress in safe RL, the benchmark should incorporate major existing works and adapt to advancements. By encompassing these pillars, the benchmark provides a solid foundation for addressing these open problems in safe RL research.

In light of the above-mentioned pillars, this paper introduces GUARD, a **G**eneralized **U**nified S**A**fe **R**einforcement Learning **D**evelopment Benchmark. In particular, GUARD is developed based upon the Safety Gym (Ray et al., 2019), SafeRL-Kit (Zhang et al., 2022a) and SpinningUp (Achiam, 2018). Unlike existing benchmarks, GUARD pushes the boundary beyond the limit by significantly extending the algorithms in comparison , types of agents and tasks, and safety constraint specifications. The contributions of this paper are as follows:

1. **Generalized benchmark with a wide range of agents.** GUARD genuinely supports **11** different agents, covering the majority of real robot types.

2. **Generalized benchmark with a wide range of locomotion tasks.** GUARD comprehensively supports **7** distinct robot locomotion task specifications, which can be combined to represent a wide spectrum of real-world robot tasks that necessitate intricate locomotion for successful completion.

3. **Generalized benchmark with a wide range of safety constraints.** GUARD genuinely supports **8** different safety constraint specifications. The included constraint options comprehensively cover the safety requirements that would encounter in real-world applications.

4. **Unified benchmarking platform with comprehensive coverage of safe RL algorithms.** Guard implements **8** state-of-the-art on-policy safe RL algorithms following a unified code structure.

5. **Highly customizable benchmarking platform.** GUARD features a modularized design that enables effortless customization of new robot locomotion testing suites with self-customizable agents, tasks, and constraints. The algorithms in GUARD are self-contained, with a consistent structure and independent implementations, ensuring clean code organization and eliminating dependencies between different algorithms. This self-contained structure greatly facilitates the seamless integration of new algorithms for further extensions.

2 Related Work

Open-source Libraries for Reinforcement Learning Algorithms Open-source RL libraries are code bases that implement representative RL algorithms for efficient deployment and comparison. They often serve as backbones for developing new RL algorithms, greatly facilitating RL research. We divide existing libraries into two categories: (a) safety-oriented RL libraries that support safe RL algorithms, and (b) general RL libraries that do not. Among safety-oriented libraries, Safety Gym (Ray et al., 2019) is the most famous one with highly configurable tasks and constraints but only supports three safe RL methods. SafeRL-Kit (Zhang et al., 2022a) supports five safe RL methods while missing some key methods such as CPO (Achiam et al., 2017). Bullet-Safety-Gym (Gronauer, 2022) supports CPO but is limited in overall safe RL support at totally four methods. Compared to the above libraries, our proposed GUARD doubles the support at eight methods in total, covering a wider spectrum of general safe RL research. General RL libraries, on the other hand, can be summarized according to their backend into PyTorch (Achiam, 2018; Weng et al., 2022; Raffin et al., 2021; Liang et al., 2018), Tensorflow (Dhariwal et al., 2017; Hill et al., 2018), Jax (Castro et al., 2018; Hoffman et al., 2020), and Keras (Plappert, 2016). In particular, SpinningUp (Achiam, 2018) serves as the major backbone of our GUARD benchmark on the safety-agnostic RL portion.

Benchmark Platform for Safe RL Algorithms To facilitate safe RL research, the benchmark platform should support a wide range of task objectives, constraints, and agent types. Among existing work, the most representative one is Safety Gym (Ray et al., 2019) which is highly configurable. However, Safety Gym is limited in agent types in that it does not support high-dimensional agents (e.g., drone and arm) and lacks

tasks with complex interactions (e.g., chase and defense). Moreover, Safety Gym only supports naive contact dynamics (e.g., touch and snap) instead of more realistic cases (e.g., objects bouncing off upon contact) in contact-rich tasks. Safe Control Gym (Yuan et al., 2022) is another open-source platform that supports very simple dynamics (i.e., cartpole, 1D/2D quadrotors) and only supports navigation tasks. Bullet Safety Gym (Gronauer, 2022) provides high-fidelity agents, but the types of agents are limited, and they only consider navigation tasks. Safety-Gymnasium (Ji et al., 2023) provides a rich array of safety RL task categories. However, it faces limitations in implementing / supporting modern safe RL algorithms and offering a flexible testing suite for each category. These weaknesses are particularly notable in the context of locomotion tasks, where there are very limited options for robots, constraints, and objectives. Compared to the above platforms, our GUARD supports a much wider range of robot locomotion task objectives (e.g., 3D reaching, chase and defense) with a much larger variety of eight agents including high-dimensional ones such as drones, arms, ants, and walkers.

3 Preliminaries

Markov Decision Process An Markov Decision Process (MDP) is specified by a tuple $(\mathcal{S}, \mathcal{A}, \gamma, \mathcal{R}, P, \rho)$, where $\mathcal{S}$ is the state space, and $\mathcal{A}$ is the control space, $\mathcal{R} : \mathcal{S} \times \mathcal{A} \to \mathbb{R}$ is the reward function, $0 \leq \gamma < 1$ is the discount factor, $\rho : \mathcal{S} \to [0, 1]$ is the starting state distribution, and $P : \mathcal{S} \times \mathcal{A} \times \mathcal{S} \to [0, 1]$ is the transition probability function (where $P(s'|s, a)$ is the probability of transitioning to state s' given that the previous state was s and the agent took action a at state s). A stationary policy $\pi : \mathcal{S} \to \mathcal{P}(\mathcal{A})$ is a map from states to a probability distribution over actions, with $\pi(a|s)$ denoting the probability of selecting action a in state s. We denote the set of all stationary policies by Π. Suppose the policy is parameterized by θ; policy search algorithms search for the optimal policy within a set $\Pi_\theta \subset \Pi$ of parameterized policies.

The solution of the MDP is a policy π that maximizes the performance measure $\mathcal{J}(\pi)$ computed via the discounted sum of reward:

$$\mathcal{J}(\pi) = \mathbb{E}_{\tau\sim\pi}\left[\sum_{t=0}^{\infty} \gamma^t \mathcal{R}(s_t, a_t, s_{t+1})\right], \tag{1}$$

where $\tau = [s_0, a_0, s_1, \cdots]$ is the state and control trajectory, and $\tau \sim \pi$ is shorthand for that the distribution over trajectories depends on $\pi : s_0 \sim \mu, a_t \sim \pi(\cdot|s_t), s_{t+1} \sim P(\cdot|s_t, a_t)$. Let $R(\tau) \doteq \sum_{t=0}^{\infty} \gamma^t \mathcal{R}(s_t, a_t, s_{t+1})$ be the discounted return of a trajectory. We define the on-policy value function as $V^\pi(s) \doteq \mathbb{E}_{\tau\sim\pi}[R(\tau)|s_0 = s]$, the on-policy action-value function as $Q^\pi(s, a) \doteq \mathbb{E}_{\tau\sim\pi}[R(\tau)|s_0 = s, a_0 = a]$, and the advantage function as $A^\pi(s, a) \doteq Q^\pi(s, a) - V^\pi(s)$.

Constrained Markov Decision Process A constrained Markov Decision Process (CMDP) is an MDP augmented with constraints that restrict the set of allowable policies. Specifically, CMDP introduces a set of cost functions, $C_1, C_2, \cdots, C_m$, where $C_i : \mathcal{S} \times \mathcal{A} \times \mathcal{S} \to \mathbb{R}$ maps the state action transition tuple into a cost value. Similar to equation 1, we denote $\mathcal{J}_{C_i}(\pi) = \mathbb{E}_{\tau\sim\pi}[\sum_{t=0}^{\infty} \gamma^t C_i(s_t, a_t, s_{t+1})]$ as the cost measure for policy π with respect to the cost function C_i. Hence, the set of feasible stationary policies for CMDP is then defined as $\Pi_C = \{\pi \in \Pi \big| \ \forall i, \mathcal{J}_{C_i}(\pi) \leq d_i\}$, where $d_i \in \mathbb{R}$. In CMDP, the objective is to select a feasible stationary policy π that maximizes the performance: $\max_{\pi\in\Pi_\theta\cap\Pi_C} \mathcal{J}(\pi)$. Lastly, we define on-policy value, action-value, and advantage functions for the cost as $V^\pi_{C_i}$, $Q^\pi_{C_i}$ and $A^\pi_{C_i}$, which as analogous to V^π, Q^π, and A^π, with C_i replacing R.

4 GUARD Safe RL Library

4.1 Overall Implementation

As a highly self contained safe RL benchmark, GUARD contains the latest methods that can achieve on-policy safe RL: (i) end-to-end safe RL algorithms including CPO (Achiam et al., 2017), TRPO-Lagrangian (Bohez et al., 2019), TRPO-FAC (Ma et al., 2021), TRPO-IPO (Liu et al., 2020), and PCPO (Yang et al., 2020); (ii) hierarchical safe RL algorithms including TRPO-SL (TRPO-Safety Layer) (Dalal et al., 2018) and TRPO-USL

(TRPO-Unrolling Safety Layer) (Zhang et al., 2022a). We also include TRPO (Schulman et al., 2015) as an unconstrained RL baseline. Note that GUARD only considers model-free approaches which rely less on assumptions than model-based ones. We highlight the benefits of our algorithm implementations in GUARD:

- GUARD comprehensively covers a **wide range of on-policy algorithms** that enforce safety in both hierarchical and end-to-end structures. Hierarchical methods maintain a separate safety layer, while end-to-end methods solve the constrained learning problem as a whole.
- GUARD provides a **fair comparison among safety components** by equipping every algorithm with the same reward-oriented RL backbone (i.e., TRPO (Schulman et al., 2015)), implementation (i.e., MLP policies with [64, 64] hidden layers and tanh activation), and training procedures. Hence, all algorithms inherit the performance guarantee of TRPO.
- GUARD is implemented in PyTorch with a clean structure where every algorithm is self-contained, enabling **fast customization and development** of new safe RL algorithms. GUARD also comes with unified logging and plotting utilities which makes analysis easy.

4.2 Unconstrained RL

TRPO We include TRPO (Schulman et al., 2015) since it is state-of-the-art and several safe RL algorithms are based on it. TRPO is an unconstrained RL algorithm and only maximizes performance $\mathcal{J}$. The key idea behind TRPO is to iteratively update the policy within a local range (trust region) of the most recent version π_k. Mathematically, TRPO updates policy via

$$\pi_{k+1} = \arg\max_{\pi \in \Pi_\theta} \mathcal{J}(\pi) \qquad \textbf{s.t.}\, \mathcal{D}_{KL}(\pi, \pi_k) \leq \delta, \tag{2}$$

where $\mathcal{D}_{KL}$ is Kullback-Leibler (KL) divergence, $\delta > 0$ and the set $\{\pi \in \Pi_\theta \ : \ \mathcal{D}_{KL}(\pi, \pi_k) \leq \delta\}$ is called the *trust region*. To solve equation 2, TRPO applies Taylor expansion to the objective and constraint at π_k to the first and second order, respectively. That results in an approximate optimization with linear objective and quadratic constraints (LOQC). TRPO guarantees a worst-case performance degradation.

4.3 End-to-End Safe RL

4.3.1 Constrained Policy Optimization-based Algorithms

CPO Constrained Policy Optimizaiton (CPO) (Achiam et al., 2017) handles CMDP by extending TRPO. Similar to TRPO, CPO also performs local policy updates in a trust region. Different from TRPO, CPO additionally requires π_{k+1} to be constrained by $\Pi_\theta \cap \Pi_C$. For practical implementation, CPO replaces the objective and constraints with surrogate functions (advantage functions), which can easily be estimated from samples collected on π_k, formally:

$$\begin{aligned} \pi_{k+1} = \arg\max_{\pi \in \Pi_\theta} & \mathop{\mathbb{E}}_{\substack{s \sim d^{\pi_k} \\ a \sim \pi}} [A^{\pi_k}(s, a)] \\ \textbf{s.t.} \quad \mathcal{D}_{KL}(\pi, \pi_k) \leq \delta, \quad & \mathcal{J}_{C_i}(\pi_k) + \frac{1}{1-\gamma} \mathop{\mathbb{E}}_{\substack{s \sim d^{\pi_k} \\ a \sim \pi}} \left[A^{\pi_k}_{C_i}(s, a) \right] \leq d_i, i = 1, \cdots, m. \end{aligned} \tag{3}$$

where $d^{\pi_k} \doteq (1-\gamma) \sum_{t=0}^{H} \gamma^t P(s_t = s | \pi_k)$ is the discounted state distribution. Following TRPO, CPO also performs Taylor expansion on the objective and constraints, resulting in a Linear Objective with Linear and Quadratic Constraints (LOLQC). CPO inherits the worst-case performance degradation guarantee from TRPO and has a worst-case cost violation guarantee.

PCPO Projection-based Constrained Policy Optimization (PCPO) (Yang et al., 2020) is proposed based on CPO, where PCPO first maximizes reward using a trust region optimization method without any constraints,

then PCPO reconciles the constraint violation (if any) by projecting the policy back onto the constraint set. Policy update then follows an analytical solution:

$$\pi_{k+1} = \pi_k + \sqrt{\frac{2\delta}{g^\top H^{-1} g}} H^{-1} g - \max\left(0, \frac{\sqrt{\frac{2\delta}{g^\top H^{-1} g}} g_c^\top H^{-1} g + b}{g_c^\top L^{-1} g_c}\right) L^{-1} g_c \tag{4}$$

where g_c is the gradient of the cost advantage function, g is the gradient of the reward advantage function, H is the Hessian of the KL divergence constraint, b is the constraint violation of the policy π_k, $L = \mathcal{I}$ for L_2 norm projection, and $L = H$ for KL divergence projection. PCPO provides a lower bound on reward improvement and an upper bound on constraint violation.

4.3.2 Lagrangian-based Algorithms

TRPO-Lagrangian Lagrangian methods solve constrained optimization by transforming hard constraints into soft constraints in the form of penalties for violations. Given the objective $\mathcal{J}(\pi)$ and constraints $\{\mathcal{J}_{C_i}(\pi) \leq d_i\}_i$, TRPO-Lagrangian (Bohez et al., 2019) first constructs the dual problem

$$\max_{\forall i, \lambda_i \geq 0} \min_{\pi \in \Pi_\theta} -\mathcal{J}(\pi) + \sum_i \lambda_i (\mathcal{J}_{C_i}(\pi) - d_i). \tag{5}$$

The update of θ is done via a trust region update with the objective of equation 2 replaced by that of equation 5 while fixing λ_i. The update of λ_i is done via standard gradient ascend. Note that TRPO-Lagrangian does not have a theoretical guarantee for constraint satisfaction.

TRPO-FAC Inspired by Lagrangian methods and aiming at enforcing state-wise constraints (e.g., preventing state from stepping into infeasible parts in the state space), Feasible Actor Critic (FAC) (Ma et al., 2021) introduces a multiplier (dual variable) network. Via an alternative update procedure similar to that for equation 5, TRPO-FAC solves the *statewise* Lagrangian objective:

$$\max_{\forall i, \xi_i} \min_{\pi \in \Pi_\theta} -\mathcal{J}(\pi) + \sum_i \mathbb{E}_{s \sim d^{\pi_k}} \left[\lambda_{\xi_i}(s)(\mathcal{J}_{C_i}(\pi) - d_i)\right], \tag{6}$$

where $\lambda_{\xi_i}(s)$ is a parameterized Lagrangian multiplier network and is parameterized by ξ_i for the i-th constraint. Note that TRPO-FAC does not have a theoretical guarantee for constraint satisfaction.

TRPO-IPO TRPO-IPO (Liu et al., 2020) incorporates constraints by augmenting the optimization objective in equation 2 with logarithmic barrier functions, inspired by the interior-point method (Boyd & Vandenberghe, 2004). Ideally, the augmented objective is $I(\mathcal{J}_{C_i}(\pi) - d_i) = 0$ if $\mathcal{J}_{C_i}(\pi) - d_i \leq 0$ or $-\infty$ otherwise. Intuitively, that enforces the constraints since the violation penalty would be $-\infty$. To make the objective differentiable, $I(\cdot)$ is approximated by $\phi(x) = \log(-x)/t$ where $t > 0$ is a hyperparameter. Then TRPO-IPO solves equation 2 with the objective replaced by $\mathcal{J}_{\text{IPO}}(\pi) = \mathcal{J}(\pi) + \sum_i \phi(\mathcal{J}_{C_i}(x) - d_i)$. TRPO-IPO does not have theoretical guarantees for constraint satisfaction.

4.4 Hierarchical Safe RL

Safety Layer Safety Layer (Dalal et al., 2018), added on top of the original policy network, conducts a quadratic-programming-based constrained optimization to project reference action into the nearest safe action. Mathematically:

$$a_t^{safe} = \arg\min_a \frac{1}{2}\|a - a_t^{ref}\|^2 \quad \textbf{s.t.} \quad \forall i, \bar{g}_{\varphi_i}(s_t)^\top a + C_i(s_{t-1}, a_{t-1}, s_t) \leq d_i \tag{7}$$

where $a_t^{ref} \sim \pi_k(\cdot|s_t)$, and $\bar{g}_{\varphi_i}(s_t)^\top a_t + C_i(s_{t-1}, a_{t-1}, s_t) \approx C_i(s_t, a_t, s_{t+1})$ is a φ parameterized linear model. If there's only one constraint, equation 7 has a closed-form solution.

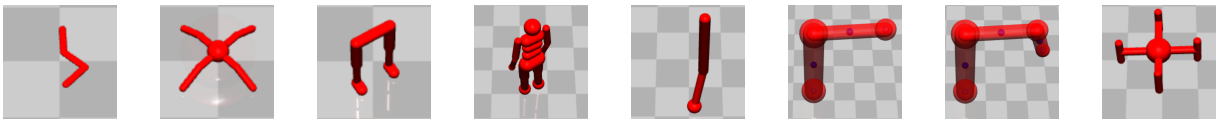

Swimmer Ant Walker Humanoid Hopper Arm3 Arm6 Drone

Figure 1: Robots of our environments.

USL Unrolling Safety Layer (USL) (Zhang et al., 2022b) is proposed to project the reference action into safe action via gradient-based correction. Specifically, USL iteratively updates the learned $Q_C(s, a)$ function with the samples collected during training. With step size η and normalization factor $\mathcal{Z}$, USL performs gradient descent as $a_t^{safe} = a_t^{ref} - \frac{\eta}{\mathcal{Z}} \cdot \frac{\partial}{\partial a_t^{ref}}[Q_C(s_t, a_t^{ref}) - d]$.

5 GUARD Testing Suite

5.1 Robot Options

In GUARD testing suite, the agent (in the form of a robot) perceives the world through sensors and interacts with the world through actuators. Robots are specified through MuJoCo XML files. The suite is equipped with **8** types of pre-made robots that we use in our benchmark environments as shown in Figure 1. The action space of the robots are continuous, and linearly scaled to [-1, +1].

Swimmer consist of three links and two joints. Each joint connects two links to form a linear chain. Swimmer can move around by applying **2** torques on the joints.

Ant is a quadrupedal robot composed a torso and four legs. Each of the four legs has a hip joint and a knee joint; and can move around by applying **8** torques to the joints.

Walker is a bipedal robot that consists of four main parts - a torso, two thighs, two legs, and two feet. Different from the knee joints and the ankle joints, each of the hip joints has three hinges in the x, y and z coordinates to help turning. With the torso height fixed, Walker can move around by controlling **10** joint torques.

Humanoid is also a bipedal robot that has a torso with a pair of legs and arms. Each leg of Humanoid consists of two joints (no ankle joint). Since we mainly focus on the navigation ability of the robots in designed tasks, the arm joints of Humanoid are fixed, which enables Humanoid to move around by only controlling **6** torques.

Hopper is a one-legged robot that consists of four main parts - a torso, a thigh, a leg, and a single foot. Similar to Walker, Hopper can move around by controlling **5** joint torques.

Arm3 is designed to simulate a fixed three-joint robot arm. Arm is equipped with multiple sensors on each links in order to fully observe the environment. By controlling **3** joint torques, Arm can move its end effector around with high flexibility.

Arm6 is designed to simulate a robot manipulator with a fixed base and six joints. Similar to Arm3, Arm6 can move its end effector around by controlling **6** torques.

Drone is designed to simulate a quadrotor. The interaction between the quadrotor and the air is simulated by applying four external forces on each of the propellers. The external forces are set to balance the gravity when the control action is zero. Drone can move in 3D space by applying **4** additional control forces on the propellers.

5.2 Task Options

We categorize robot tasks in two ways: (i) interactive versus non-interactive tasks, and (ii) 2D space versus 3D space tasks. 2D space tasks constrain agents to a planar space, while 3D space tasks do not. Non-interactive tasks primarily involve achieving a target state (e.g., trajectory tracking) while interactive tasks (e.g., human-

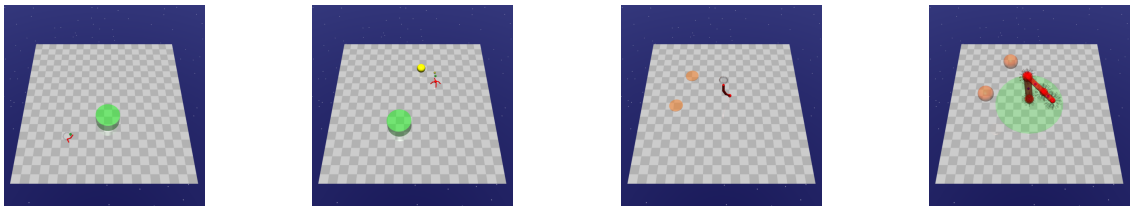

(a) Goal (b) Push (c) Chase (d) Defense

Figure 2: Tasks of our environments.

robot collaboration and unstructured object pickup) necessitate contact or non-contact interactions between the robot and humans or movable objects, rendering them more challenging. On a variety of tasks that cover different situations, GUARD facilitates a thorough evaluation of safe RL algorithms via the following tasks. See Table 17 for more information.

Goal (Figure 2a) requires the robot navigating towards a series of 2D or 3D goal positions. Upon reaching a goal, the location is randomly reset. The task provides a sparse reward upon goal achievement and a dense reward for making progress toward the goal.

Push (Figure 2b) requires the robot pushing a ball toward different goal positions. The task includes a sparse reward for the ball reaching the goal circle and a dense reward that encourages the agent to approach both the ball and the goal. Unlike pushing a box in Safety Gym, it is more challenging to push a ball since the ball can roll away and the contact dynamics are more complex.

Chase (Figure 2c) requires the robot tracking multiple dynamic targets. Those targets continuously move away from the robot at a slow speed. The dense reward component provides a bonus for minimizing the distance between the robot and the targets. The targets are constrained to a circular area. A 3D version of this task is also available, where the targets move within a restricted 3D space. Detailed dynamics of the targets is described in Appendix B.5.1.

Defense (Figure 2d) requires the robot to prevent dynamic targets from entering a protected circle area. The targets will head straight toward the protected area or avoid the robot if the robot gets too close. Dense reward component provides a bonus for increasing the cumulative distance between the targets and the protected area. Detailed dynamics of the targets is described in Appendix B.5.2.

5.3 Constraint Options

We classify constraints based on various factors: **trespassibility**: whether constraints are trespassable or untrespassable. Trespassable constraints allow violations without causing any changes to the robot's behaviors, and vice versa. (ii) **movability**: whether they are immovable, passively movable, or actively movable; and (iii) **motion space**: whether they pertain to 2D or 3D environments. To cover a comprehensive range of constraint configurations, we introduce additional constraint types via expanding Safety Gym. Please refer to Table 18 for all configurable constraints.

3D Hazards (Figure 3a) are dangerous 3D areas to avoid. These are floating spheres that are trespassable, and the robot is penalized for entering them.

Ghosts (Figure 3b) are dangerous areas to avoid. Different from hazards, ghosts always move toward the robot slowly, represented by circles on the ground. Ghosts can be either trespassable or untrespassable. The robot is penalized for touching the untrespassable ghosts and entering the trespassable ghosts. Moreover, ghosts can be configured to start chasing the robot when the distance from the robot is larger than some threshold. This feature together with the adjustable velocity allows users to design the ghosts with different aggressiveness. Detailed dynamics of the targets is described in Appendix B.5.3.

3D Ghosts (Figure 3c) are dangerous 3D areas to avoid. These are floating spheres as 3D version of ghosts, sharing the similar behaviour with ghosts.

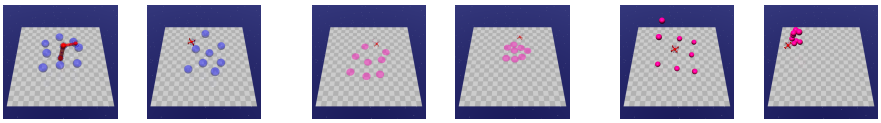

(a) 3D Hazards (b) Ghosts (c) 3D Ghosts

Figure 3: Constraints of our environments.

6 GUARD Experiments

In our experiments, we aim to answer these questions:

Q1 What are the overall benchmark results?

Q2 What are the impacts of constraint difficulty on algorithm performance?

Q3 What are the characteristics of different categories of safe RL algorithm?

Q4 What are the impacts of task complexity on algorithm performance?

Q5 How does adaptive multiplier impact Lagrangian-based methods?

Q6 How does feasibility projection impact CPO-based methods?

Q7 How does cost dynamics linearization impact Hierarchical-based methods?

Q8 What is the individual algorithm performance across all tasks?

6.1 Experiment Setup

In GUARD experiments, our objective is to assess the performance of safe RL algorithms across a diverse range of benchmark testing suites. These suites are meticulously designed, incorporating all available robot options as detailed in Section 5.1 and all task options outlined in Section 5.2. Additionally, we offer seamless integration of various constraint options into these benchmark testing suites, allowing users to select desired constraint types, numbers, sizes, and other parameters. Considering the diversity in robots, tasks, constraint types, and difficulty levels, we have curated 72 test suites. These predefined benchmark testing suites follow the format `{Task}_{Robot}_{Constraint Number}{Constraint Type}`. For a comprehensive list of our testing suites, please refer to Table 20.

Comparison Group The methods in the comparison group include all methods in GUARD Safe RL Libraray: (i) unconstrained RL algorithm TRPO (Schulman et al., 2015) (ii) end-to-end constrained safe RL algorithms CPO (Achiam et al., 2017), TRPO-Lagrangian (Bohez et al., 2019), TRPO-FAC (Ma et al., 2021), TRPO-IPO (Liu et al., 2020), PCPO (Yang et al., 2020), and (iii) hierarchical safe RL algorithms TRPO-SL (TRPO-Safety Layer) (Dalal et al., 2018), TRPO-USL (TRPO-Unrolling Safety Layer) (Zhang et al., 2022a). For hierarchical safe RL algorithms, we incorporate a warm-up phase (constituting 1/3 of the total epochs) dedicated to unconstrained TRPO training. The data generated during this phase is utilized to pre-train the safety critic for subsequent epochs. The target cost for all safe RL methods is set to zero, aligning with our objective of achieving zero violations. To ensure consistency, shared configurations, including hidden layers, learning rate, and target KL, are uniformly applied across all methods. Simultaneously, unique parameters such as Lagrangian learning rate, IPO parameter, and Warmup ratio are fine-tuned to optimize the performance of each respective method. Further details are provided in Table 19.

6.2 Evaluating GUARD Safe RL Library and Comparison Analysis

Overall Benchmark Results The summarized results can be found in Tables 21 to 25, and the learning rate curves are presented in Figures 13 to 17. As shown in Figure 4, we select 8 set of results to demonstrate the performance of different robot, task and constraints in GUARD. At a high level, the experiments show that all methods can consistently improve reward performance.

Different methods have different trade-offs between rewards and cost. When comparing constrained RL methods to unconstrained RL methods, the former exhibit superior performance in terms of cost reduction. By incorporating constraints into the RL framework, the robot can navigate its environment while minimizing costs. This feature is particularly crucial for real-world applications where the avoidance of hazards and obstacles is of utmost importance. However, current safe RL algorithms (i.e. CPO, PCPO and Lagrangian methods) are hard to achieve zero-violation performance even when the cost threshold is set as zero. Comparing with them, hierarchical RL methods (i.e., TRPO-SL and TRPO-USL) can perform better at cost reduction. Nevertheless, although these methods excel at minimizing costs, they may sacrifice some degree of reward attainment in the process.

Impacts of Constraints Difficulty To assess the impact of constraint difficulty on the performance of various safe RL algorithms, we analyze the performance changes across different algorithms using the `Goal_Point_8{Constraint}` testing suites. Specifically, we vary `8{Constraint}` from `8Hazards` to `8Ghosts`, with the former representing an easier constraint where all hazards are static, and the latter indicating a more challenging constraint where all hazards are adversarially moving towards the robot. To ensure a fair comparison across diverse tasks, we report the normalized reward and normalized cost for each algorithm using the following metric:

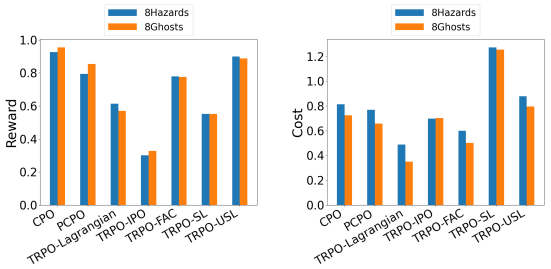

Figure 5: constraint difficulty ablation study with Goal_Point_8{Constraint}

$$reward_{normalized} = \min\left(\frac{reward_{algorithm}}{reward_{TRPO}}, 1\right) \tag{8}$$

$$cost_{normalized} = \frac{cost_{algorithm}}{cost_{TRPO}} \tag{9}$$

where $reward_{normalized}$ are obtained from Tables 21 to 25. Before applying Equation (8), in cases where negative values exist for $reward_{normalized}$ in the results, we shift all values to be above zero with respect to the minimum $reward_{normalized}$ observed within the same experiment.

The comparative results are succinctly presented in Figure 5. Notably, as the constraint difficulty transitions from an easier to a more challenging level, majority algorithms within the Safe RL Library showcase safer policy learning behaviors. Additionally, they manage to maintain roughly the same, and in some instances, achieve higher reward performance. This observation underscores two key findings: (i) safe RL algorithms exhibit resilience to the increased difficulty of constraints, and (ii) heightened constraint difficulty serves as a more effective metric for distinguishing safety performance. Notably, the cost performance gap between TRPO-Lagrangian and TRPO-IPO is magnified in the Ghost environment, where a more sophisticated safe policy is in need to avoid adversarial hazards.

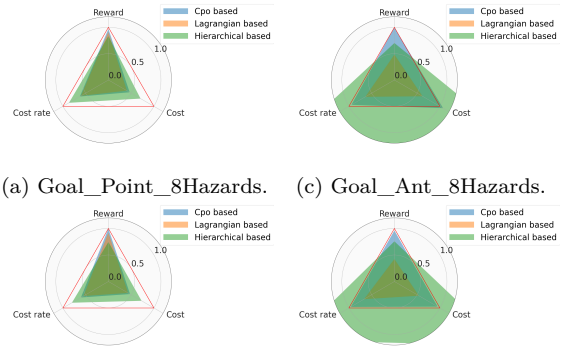

(a) Goal_Point_8Hazards. (c) Goal_Ant_8Hazards.

(b) Goal_Point_8Ghosts. (d) Goal_Ant_8Ghosts.

Figure 6: Comparison of algorithm categories in four representative test suites across low-to-high dimensional robots and easy-to-hard constraints.

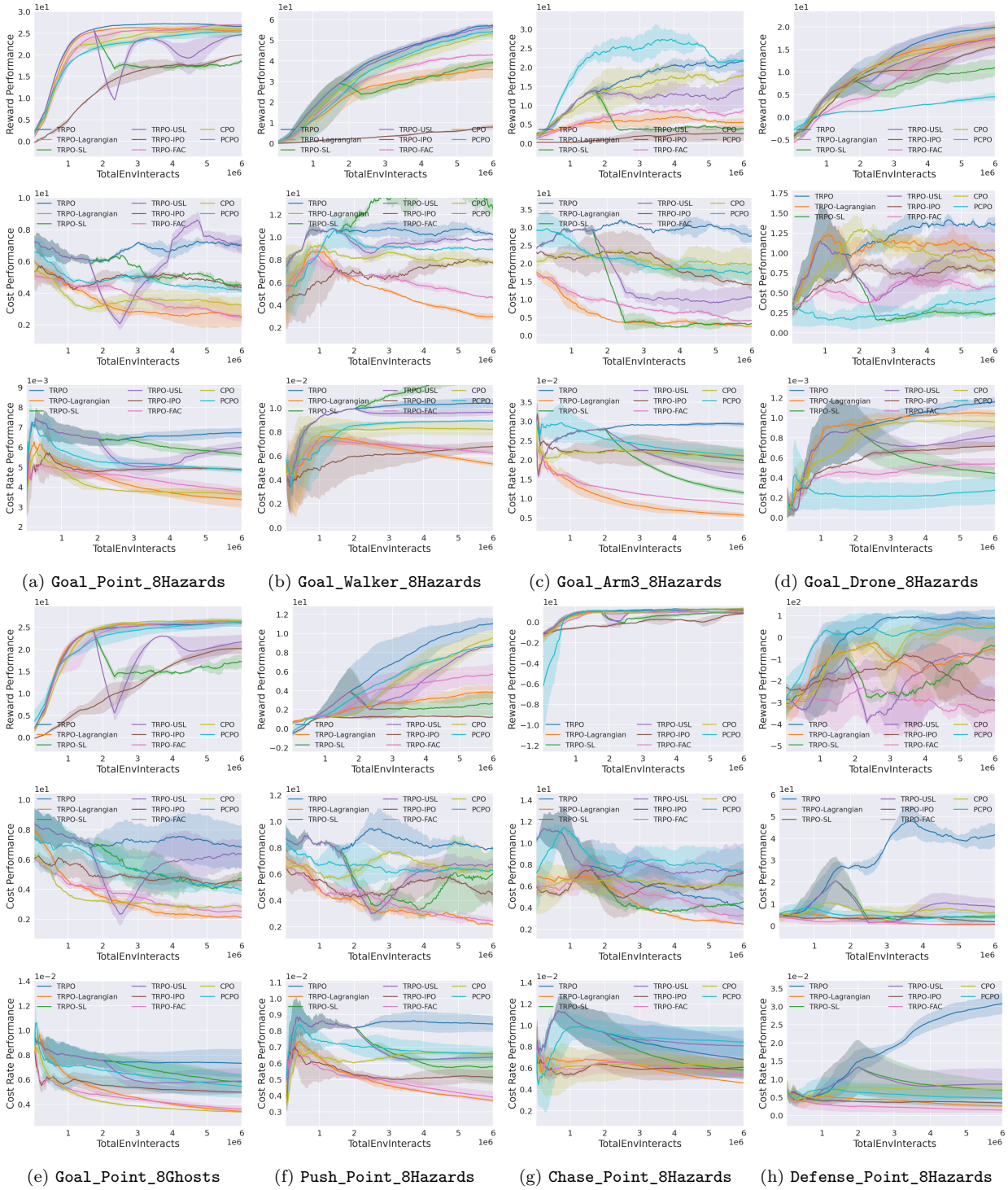

(a) `Goal_Point_8Hazards` (b) `Goal_Walker_8Hazards` (c) `Goal_Arm3_8Hazards` (d) `Goal_Drone_8Hazards`

(e) `Goal_Point_8Ghosts` (f) `Push_Point_8Hazards` (g) `Chase_Point_8Hazards` (h) `Defense_Point_8Hazards`

Figure 4: Comparison of results from four representative tasks. (a) to (d) cover four robots on the goal task. (e) shows the performance of a task with ghosts. (f) to (h) cover three different tasks with the point robot.

Characteristics of Different Categories of Safe RL Algorithms Within the Safe RL Library, three primary categories of safe RL algorithms exist: (i) Lagrangian-based methods (TRPO-Lagrangian, TRPO-FAC, TRPO-IPO), (ii) constrained policy optimization-based methods (CPO, PCPO), and (iii) hierarchical-based methods (Safe Layer, USL). To investigate the performance characteristics inherent in each category, we carefully select four representative testing suites spanning high/low dimensional robots and easy/hard constraints. Subsequently, we chart the algorithm-wise averaged TRPO normalized reward, cost, and cost rate. For example, the algorithm-wise averaged score for hierarchical-based methods is computed by taking the mean across Safe Layer and USL. Additionally, the TRPO normalized cost rate is defined as:

$$cost\ rate_{normalized} = \frac{cost\ rate_{algorithm}}{cost\ rate_{TRPO}} \tag{10}$$

The summarized comparison results are presented in fig. 6. Generally, in terms of safety performance, Lagrangian-based methods demonstrate the highest efficacy, followed by CPO-based methods, while Hierarchical-based methods exhibit comparatively lower performance. Several key observations emerge: (i) Lagrangian-based methods prioritize safety performance and are willing to make concessions in reward performance when necessary, as evidenced by significantly lower reward performance in high-dimensional tasks. (ii) CPO-based methods tend to maintain a high standard of reward performance akin to unconstrained RL, but this strategy compromises safe behavior, particularly in high-dimensional tasks. (iii) Hierarchical-based methods only demonstrate effectiveness in low-dimensional systems, struggling to learn reasonable safe behavior in high-dimensional systems. This limitation is attributed to the escalating complexity of cost function dynamics in high-dimensional systems, posing challenges for effective cost function approximation.

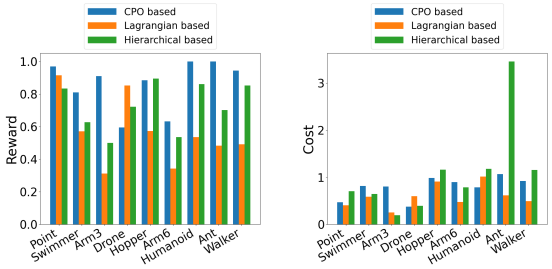

Figure 7: TRPO normalized performance metrics (Reward and Cost) of three algorithm categories across varied difficulty levels in Goal_{Robot}_8Hazards

Effects of Task Complexity on Various Categories of Safe RL Algorithms To examine the impact of increased task complexity, particularly in the context of higher degrees of freedom (DOF) in robots, we summarize the TRPO normalized performance metrics (reward and cost) for three algorithm categories across various difficulty levels in the Goal_{Robot}_8Hazards testing suites, with an incremental increase in robot DOF, in Figure 7. The performance characteristics of different algorithm categories exhibit interesting variations with heightened task complexity.

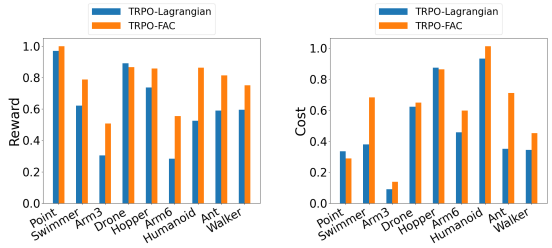

Figure 8: TRPO normalized performance metrics (Reward and Cost) of Lagrangian and FAC across varied difficulty levels in Goal_{Robot}_8Hazards

Surprisingly, there is no discernible trend in reward and cost performance across all algorithm categories as task complexity increases. However, Lagrangian and Hierarchical-based methods each align better with specific robot types. (i) For Arm robots, Lagrangian-based methods struggle to learn reward, whereas Hierarchical-based methods perform well on both reward and safety. (ii) In the case of linked/legged robots, Lagrangian-based methods maintain a consistent, albeit mediocre, reward performance, coupled with optimal safety performance. Conversely, Hierarchical-based methods struggle to learn a safe policy, particularly on the Ant robot.

Regarding CPO-based methods, their reward performance remains consistently high even with increased task complexity. However, although CPO-based methods exhibit effective learning of safe policies with low-dimensional robots, they encounter difficulties in learning optimal safe behavior as task complexity exceeds certain threshold.

Impacts of Adaptive Multiplier in Lagrangian-based Methods An essential differentiator between TRPO-FAC and TRPO-Lagrangian lies in the incorporation of a multiplier network, i.e. an adaptive multiplier. To gain a comprehensive understanding of this technique, we compare the normalized performance metrics on Goal_{Robot}_8Hazards testing suites, both with and without this feature, as illustrated in Figure 8. It is evident that the introduction of the adaptive multiplier results in consistently stable and favorable performance across various difficulty levels of tasks. However, as a trade-off, the adaptive multiplier tends to compromise safety performance, leading to higher costs, particularly evident in Swimmer and Ant.

Impacts of Feasibility Projection in CPO-based Methods The policy rule of PCPO enhances CPO by projecting the reward-oriented policy back into the constraint set, ensuring a feasible policy update at every iteration (feasibility projection). To assess the impact of this technique, we conduct a comparison of normalized performance metrics on Goal_{Robot}_8Hazards testing suites, both with and without this feature, as depicted in Figure 9. The figure indicates that feasibility projection is potent in trading off performance for significantly safer behavior in specific tasks, such as the Drone task. However, this may not be universally applicable, as feasibility projection often leads to slightly less safe behavior and, in some cases, adversely affects reward performance without corresponding improvements in safety, as observed in the Arm6 scenario.

Impacts of Linearized Cost Dynamics Hierarchical methods offer the explicit projection of an unsafe reference action into a safe action set, a process that involves determining the cost given a state-action pair. While one approach involves directly learning the cost function, as seen in USL, SafeLayer streamlines the process by linearizing the cost function dynamics and focusing solely on learning the gradient. To assess the effectiveness of this method, we conduct a comparison of normalized performance metrics on Goal_{Robot}_8Hazards testing suites, both with and without this feature, as depicted in Figure 10. The results reveal that the linearization is highly effective in achieving robust safe behavior in low-dimensional robot tasks, particularly evident in the cases of Drone and Arm3. However, the linear approximation of the cost function in SafeLayer becomes less accurate in scenarios with highly nonlinear dynamics, such as the complex Ant robot, leading to a significant increase in overall costs. Therefore, Linearization emerges as a powerful technique for tasks with low complexity, especially those involving low-dimensional robots.

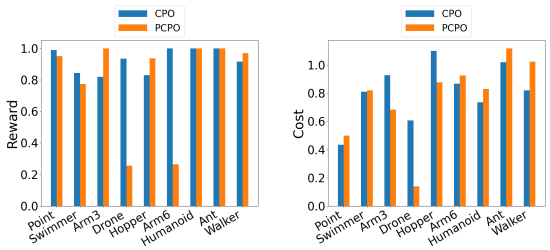

Figure 9: TRPO normalized performance metrics (Reward and Cost) of CPO and PCPO across varied difficulty levels in Goal_{Robot}_8Hazards

Lastly, for a holistic understanding of the performance exhibited by each algorithm within the Safe RL Library across all tasks within the GUARD Testing suites, we present spider plots in Figure 11. These plots illustrate the TRPO normalized reward, cost, and cost rate for each algorithm across five task options, with all performance metrics averaged over all available robot options. TRPO is utilized as the baseline in this figure, emphasizing its focus on maximizing reward performance.

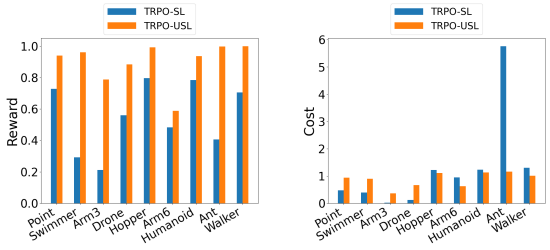

Figure 10: TRPO normalized performance metrics (Reward and Cost) of USL and SafeLayer across varied difficulty levels in Goal_{Robot}_8Hazards

Within the category of CPO-based methods: (i) CPO maintains reward levels comparable to TRPO across all tasks but struggles to learn a safe policy in the Chase task. (ii) PCPO exhibits a lower performance in both reward and safety aspects, particularly in Chase and Defense tasks.

Within the category of Lagrangian-based methods: (i) Lagrangian maintains a balance between good reward and cost across all tasks, although its reward performance is not exceptional. (ii) FAC excels in achieving

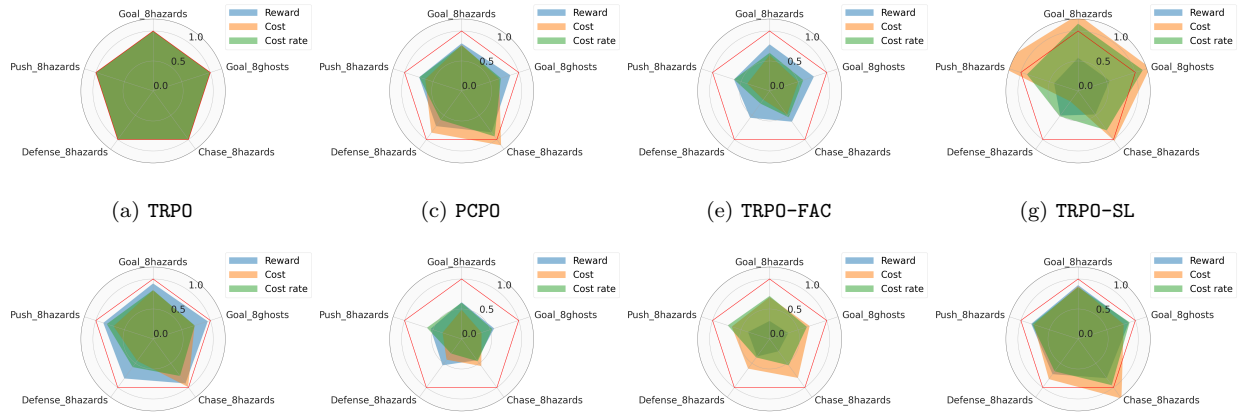

(a) TRPO (c) PCPO (e) TRPO-FAC (g) TRPO-SL

(b) CPO (d) TRPO-Lagrangian (f) TRPO-IPO (h) TRPO-USL

Figure 11: Algorithm performance over different tasks

higher reward across all tasks, with a slight sacrifice in safety performance in all tasks except Defense. (iii) IPO performs the worst in both reward and safety metrics, although it still manages to learn viable safe policies for all tasks.

Within the category of Hierarchical-based methods: (i) USL performs admirably in achieving satisfactory rewards for all tasks but only learns mediocre safe policies and struggles with the Chase task. (ii) SafeLayer demonstrates poor performance in reward performance and consistently fails to learn safe policies in most tasks. However, it excels in achieving satisfactory safety performance, particularly in the Defense task.

7 Conclusions

This paper introduces GUARD, the **G**eneralized **U**nified S**A**fe **R**einforcement Learning **D**evelopment Benchmark. GUARD offers several advantages over existing benchmarks. Firstly, it provides a generalized framework with a wide range of RL agents, tasks, and constraint specifications. Secondly, GUARD has self-contained implementations of a comprehensive range of state-of-the-art safe RL algorithms. Lastly, GUARD is highly customizable, allowing researchers to tailor tasks and algorithms to specific needs. Using GUARD, we present a comparative analysis of state-of-the-art safe RL algorithms across various task settings, establishing essential baselines for future research.

Future work In our future endeavors, we aim to address the following limitations: (i) To enhance the ease of deploying Reinforcement Learning (RL) methods on real robots, we are actively incorporating additional realistic robot models into GUARD. (ii) The current GUARD tasks primarily focus on robot locomotion; however, we are planning to broaden the spectrum of available task types to empower users with a more extensive testing suite, including options such as speed control and contact-rich safety. (iii) Lastly, we plan to extend the range of safe RL library to include the latest algorithms such as off-policy methods.

References

Joshua Achiam. Spinning Up in Deep Reinforcement Learning. 2018.

Joshua Achiam, David Held, Aviv Tamar, and Pieter Abbeel. Constrained policy optimization. In *International conference on machine learning*, pp. 22–31. PMLR, 2017.

Forest Agostinelli, Stephen McAleer, Alexander Shmakov, and Pierre Baldi. Solving the rubik's cube with deep reinforcement learning and search. *Nature Machine Intelligence*, pp. 1–8, 2019.

Steven Bohez, Abbas Abdolmaleki, Michael Neunert, Jonas Buchli, Nicolas Heess, and Raia Hadsell. Value constrained model-free continuous control. *arXiv preprint arXiv:1902.04623*, 2019.

Stephen P Boyd and Lieven Vandenberghe. *Convex optimization*. Cambridge university press, 2004.

Greg Brockman, Vicki Cheung, Ludwig Pettersson, Jonas Schneider, John Schulman, Jie Tang, and Wojciech Zaremba. Openai gym. *arXiv preprint arXiv:1606.01540*, 2016.

Lukas Brunke, Melissa Greeff, Adam W. Hall, Zhaocong Yuan, Siqi Zhou, Jacopo Panerati, and Angela P. Schoellig. Safe learning in robotics: From learning-based control to safe reinforcement learning. *Annual Review of Control, Robotics, and Autonomous Systems*, 5(1):411–444, 2022.

Pablo Samuel Castro, Subhodeep Moitra, Carles Gelada, Saurabh Kumar, and Marc G. Bellemare. Dopamine: A Research Framework for Deep Reinforcement Learning. 2018. URL `http://arxiv.org/abs/1812.06110`.

Rui Chen, Alvin Shek, and Changliu Liu. Robust and context-aware real-time collaborative robot handling via dynamic gesture commands. *IEEE Robotics and Automation Letters*, 2023.

Gal Dalal, Krishnamurthy Dvijotham, Matej Vecerik, Todd Hester, Cosmin Paduraru, and Yuval Tassa. Safe exploration in continuous action spaces. *CoRR*, abs/1801.08757, 2018.

Prafulla Dhariwal, Christopher Hesse, Oleg Klimov, Alex Nichol, Matthias Plappert, Alec Radford, John Schulman, Szymon Sidor, Yuhuai Wu, and Peter Zhokhov. Openai baselines. `https://github.com/openai/baselines`, 2017.

Yan Duan, Xi Chen, Rein Houthooft, John Schulman, and Pieter Abbeel. Benchmarking deep reinforcement learning for continuous control. In *International conference on machine learning*, pp. 1329–1338. PMLR, 2016.

Gabriel Dulac-Arnold, Nir Levine, Daniel J. Mankowitz, Jerry Li, Cosmin Paduraru, Sven Gowal, and Todd Hester. An empirical investigation of the challenges of real-world reinforcement learning. 2020.

Benjamin Ellenberger. Pybullet gymperium. `https://github.com/benelot/pybullet-gym`, 2018–2019.

Javier Garcıa and Fernando Fernández. A comprehensive survey on safe reinforcement learning. *Journal of Machine Learning Research*, 16(1):1437–1480, 2015.

Sven Gronauer. Bullet-safety-gym: A framework for constrained reinforcement learning. Technical report, TUM Department of Electrical and Computer Engineering, Jan 2022.

Shangding Gu, Guang Chen, Lijun Zhang, Jing Hou, Yingbai Hu, and Alois Knoll. Constrained reinforcement learning for vehicle motion planning with topological reachability analysis. *Robotics*, 11(4), 2022a.

Shangding Gu, Long Yang, Yali Du, Guang Chen, Florian Walter, Jun Wang, Yaodong Yang, and Alois Knoll. A review of safe reinforcement learning: Methods, theory and applications. *arXiv preprint arXiv:2205.10330*, 2022b.

Ashley Hill, Antonin Raffin, Maximilian Ernestus, Adam Gleave, Anssi Kanervisto, Rene Traore, Prafulla Dhariwal, Christopher Hesse, Oleg Klimov, Alex Nichol, Matthias Plappert, Alec Radford, John Schulman, Szymon Sidor, and Yuhuai Wu. Stable baselines. `https://github.com/hill-a/stable-baselines`, 2018.

Matthew W. Hoffman, Bobak Shahriari, John Aslanides, Gabriel Barth-Maron, Nikola Momchev, Danila Sinopalnikov, Piotr Stańczyk, Sabela Ramos, Anton Raichuk, Damien Vincent, Léonard Hussenot, Robert Dadashi, Gabriel Dulac-Arnold, Manu Orsini, Alexis Jacq, Johan Ferret, Nino Vieillard, Seyed Kamyar Seyed Ghasemipour, Sertan Girgin, Olivier Pietquin, Feryal Behbahani, Tamara Norman, Abbas Abdolmaleki, Albin Cassirer, Fan Yang, Kate Baumli, Sarah Henderson, Abe Friesen, Ruba Haroun, Alex Novikov, Sergio Gómez Colmenarejo, Serkan Cabi, Caglar Gulcehre, Tom Le Paine, Srivatsan Srinivasan, Andrew Cowie, Ziyu Wang, Bilal Piot, and Nando de Freitas. Acme: A research framework for distributed reinforcement learning. *arXiv preprint arXiv:2006.00979*, 2020. URL `https://arxiv.org/abs/2006.00979`.

David Isele, Alireza Nakhaei, and Kikuo Fujimura. Safe reinforcement learning on autonomous vehicles. *arXiv preprint arXiv:1910.00399*, 2019.

Jiaming Ji, Borong Zhang, Xuehai Pan, Jiayi Zhou, Juntao Dai, and Yaodong Yang. Safety-gymnasium. *GitHub repository*, 2023.

B Ravi Kiran, Ibrahim Sobh, Victor Talpaert, Patrick Mannion, Ahmad A. Al Sallab, Senthil Yogamani, and Patrick Pérez. Deep reinforcement learning for autonomous driving: A survey. *IEEE Transactions on Intelligent Transportation Systems*, 23(6):4909–4926, 2022.

Jens Kober, J. Andrew Bagnell, and Jan Peters. Reinforcement learning in robotics: A survey. *The International Journal of Robotics Research*, 32(11):1238–1274, 2013.

Eric Liang, Richard Liaw, Robert Nishihara, Philipp Moritz, Roy Fox, Ken Goldberg, Joseph E. Gonzalez, Michael I. Jordan, and Ion Stoica. RLlib: Abstractions for distributed reinforcement learning. In *International Conference on Machine Learning (ICML)*, 2018.

Yongshuai Liu, Jiaxin Ding, and Xin Liu. Ipo: Interior-point policy optimization under constraints. In *Proceedings of the AAAI conference on artificial intelligence*, volume 34, pp. 4940–4947, 2020.

Haitong Ma, Yang Guan, Shegnbo Eben Li, Xiangteng Zhang, Sifa Zheng, and Jianyu Chen. Feasible actor-critic: Constrained reinforcement learning for ensuring statewise safety. *arXiv preprint arXiv:2105.10682*, 2021.

Volodymyr Mnih, Koray Kavukcuoglu, David Silver, Alex Graves, Ioannis Antonoglou, Daan Wierstra, and Martin Riedmiller. Playing atari with deep reinforcement learning. *arXiv preprint arXiv:1312.5602*, 2013.

OpenAI, :, Christopher Berner, Greg Brockman, Brooke Chan, Vicki Cheung, Przemysław Dębiak, Christy Dennison, David Farhi, Quirin Fischer, Shariq Hashme, Chris Hesse, Rafal Józefowicz, Scott Gray, Catherine Olsson, Jakub Pachocki, Michael Petrov, Henrique P. d. O. Pinto, Jonathan Raiman, Tim Salimans, Jeremy Schlatter, Jonas Schneider, Szymon Sidor, Ilya Sutskever, Jie Tang, Filip Wolski, and Susan Zhang. Dota 2 with large scale deep reinforcement learning. *arXiv preprint arXiv:1912.06680*, 2019.

Ian Osband, Yotam Doron, Matteo Hessel, John Aslanides, Eren Sezener, Andre Saraiva, Katrina McKinney, Tor Lattimore, Csaba Szepesvári, Satinder Singh, Benjamin Van Roy, Richard Sutton, David Silver, and Hado van Hasselt. Behaviour suite for reinforcement learning. In *International Conference on Learning Representations*, 2020.

Matthias Plappert. keras-rl. `https://github.com/keras-rl/keras-rl`, 2016.

Ivaylo Popov, Nicolas Heess, Timothy Lillicrap, Roland Hafner, Gabriel Barth-Maron, Matej Vecerik, Thomas Lampe, Yuval Tassa, Tom Erez, and Martin Riedmiller. Data-efficient deep reinforcement learning for dexterous manipulation. *arXiv preprint arXiv:1704.03073*, 2017.

Antonin Raffin, Ashley Hill, Adam Gleave, Anssi Kanervisto, Maximilian Ernestus, and Noah Dormann. Stable-baselines3: Reliable reinforcement learning implementations. *Journal of Machine Learning Research*, 22(268):1–8, 2021. URL `http://jmlr.org/papers/v22/20-1364.html`.

Alex Ray, Joshua Achiam, and Dario Amodei. Benchmarking safe exploration in deep reinforcement learning. *CoRR*, abs/1910.01708, 2019.

John Schulman, Sergey Levine, Pieter Abbeel, Michael Jordan, and Philipp Moritz. Trust region policy optimization. In *International conference on machine learning*, pp. 1889–1897. PMLR, 2015.

Alvin Shek, Rui Chen, and Changliu Liu. Learning from physical human feedback: An object-centric one-shot adaptation method. *arXiv preprint arXiv:2203.04951*, 2022.

David Silver, Thomas Hubert, Julian Schrittwieser, Ioannis Antonoglou, Matthew Lai, Arthur Guez, Marc Lanctot, Laurent Sifre, Dharshan Kumaran, Thore Graepel, et al. A general reinforcement learning algorithm that masters chess, shogi, and go through self-play. *Science*, 362(6419):1140–1144, 2018.

Saran Tunyasuvunakool, Alistair Muldal, Yotam Doron, Siqi Liu, Steven Bohez, Josh Merel, Tom Erez, Timothy Lillicrap, Nicolas Heess, and Yuval Tassa. dm_control: Software and tasks for continuous control. *Software Impacts*, 6:100022, 2020.

Oriol Vinyals, Igor Babuschkin, Junyoung Chung, Michael Mathieu, Max Jaderberg, Wojtek Czarnecki, Andrew Dudzik, Aja Huang, Petko Georgiev, Richard Powell, Timo Ewalds, Dan Horgan, Manuel Kroiss, Ivo Danihelka, John Agapiou, Junhyuk Oh, Valentin Dalibard, David Choi, Laurent Sifre, Yury Sulsky, Sasha Vezhnevets, James Molloy, Trevor Cai, David Budden, Tom Paine, Caglar Gulcehre, Ziyu Wang, Tobias Pfaff, Toby Pohlen, Dani Yogatama, Julia Cohen, Katrina McKinney, Oliver Smith, Tom Schaul, Timothy Lillicrap, Chris Apps, Koray Kavukcuoglu, Demis Hassabis, and David Silver. AlphaStar: Mastering the Real-Time Strategy Game StarCraft II. `https://deepmind.com/blog/alphastar-mastering-real-time-strategy-game-starcraft-ii/`, 2019.

Jiayi Weng, Huayu Chen, Dong Yan, Kaichao You, Alexis Duburcq, Minghao Zhang, Yi Su, Hang Su, and Jun Zhu. Tianshou: A highly modularized deep reinforcement learning library. *Journal of Machine Learning Research*, 23(267):1–6, 2022. URL `http://jmlr.org/papers/v23/21-1127.html`.

Tsung-Yen Yang, Justinian Rosca, Karthik Narasimhan, and Peter J Ramadge. Projection-based constrained policy optimization. *arXiv preprint arXiv:2010.03152*, 2020.

Tianhe Yu, Deirdre Quillen, Zhanpeng He, Ryan Julian, Karol Hausman, Chelsea Finn, and Sergey Levine. Meta-world: A benchmark and evaluation for multi-task and meta reinforcement learning. In *Conference on Robot Learning (CoRL)*, 2019.

Zhaocong Yuan, Adam W. Hall, Siqi Zhou, Lukas Brunke, Melissa Greeff, Jacopo Panerati, and Angela P. Schoellig. Safe-control-gym: A unified benchmark suite for safe learning-based control and reinforcement learning in robotics. *IEEE Robotics and Automation Letters*, 7(4):11142–11149, 2022. doi: 10.1109/LRA.2022.3196132.

Linrui Zhang, Qin Zhang, Li Shen, Bo Yuan, and Xueqian Wang. Saferl-kit: Evaluating efficient reinforcement learning methods for safe autonomous driving. *arXiv preprint arXiv:2206.08528*, 2022a.

Linrui Zhang, Qin Zhang, Li Shen, Bo Yuan, Xueqian Wang, and Dacheng Tao. Evaluating model-free reinforcement learning toward safety-critical tasks. *arXiv preprint arXiv:2212.05727*, 2022b.

Weiye Zhao, Tairan He, Rui Chen, Tianhao Wei, and Changliu Liu. State-wise safe reinforcement learning: A survey. *The 32nd International Joint Conference on Artificial Intelligence (IJCAI)*, 2023.

A Appendix

B Environment Details

B.1 Observation Space and Action space of different robots

The action space and observation space of different robots are summarized in Tables 1 to 16

Table 1: Action space of Swimmer

Num	Action	Min	Max	Name in XML	Joint	Unit
0	Torque applied on the first rotor	-1	1	motor1_rot	hinge	torque (Nm)
1	Torque applied on the second rotor	-1	1	motor2_rot	hinge	torque (Nm)

Table 2: Observation space of Swimmer

Num	Observation	Min	Max	Name in XML	Joint	Unit
0/1/2	3-axis linear acceleration of the torso (including gravity)	-Inf	Inf	accelerometer	free	acceleration (m/s^2)
3/4/5	3-axis linear velocity of the torso	-Inf	Inf	velocimeter	free	velocity (m/s)
6/7/8	3-axis angular velocity velocity of the torso	-Inf	Inf	gyro	free	angular velocity (rad/s)
9/10/11	3D magnetic flux vector at the torso	-Inf	Inf	magnetometer	free	magnetic flux density (T)
12	Contact force at the first tip	0	Inf	touch_point1	-	force(N)
13	Contact force at the first rotor	0	Inf	touch_point2	-	force(N)
14	Contact force at the second rotor	0	Inf	touch_point3	-	force(N)
15	Contact force at the second tip	0	Inf	touch_point4	-	force(N)
16	Angle of the first rotor	-Inf	Inf	jointpos_motor1_rot	hinge	angle (rad)
17	Angle of the second rotor	-Inf	Inf	jointpos_motor2_rot	hinge	angle (rad)
18	Angular velocity of the first rotor	-Inf	Inf	jointvel_motor1_rot	hinge	angular velocity (rad/s)
19	Angular velocity of the second rotor	-Inf	Inf	jointvel_motor2_rot	hinge	angular velocity (rad/s)

Table 3: Action space of Ant

Num	Action	Min	Max	Name in XML	Joint	Unit
0	Torque applied on the rotor between the torso and front left hip	-1	1	hip_1	hinge	torque (Nm)
1	Torque applied on the rotor between the front left two links	-1	1	ankle_1	hinge	torque (Nm)
2	Torque applied on the rotor between the torso and front right hip	-1	1	hip_2	hinge	torque (Nm)
3	Torque applied on the rotor between the front right two links	-1	1	ankle_2	hinge	torque (Nm)
4	Torque applied on the rotor between the torso and back left hip	-1	1	hip_3	hinge	torque (Nm)
5	Torque applied on the rotor between the back left two links	-1	1	ankle_3	hinge	torque (Nm)
6	Torque applied on the rotor between the torso and back right hip	-1	1	hip_4	hinge	torque (Nm)
7	Torque applied on the rotor between the back right two links	-1	1	ankle_4	hinge	torque (Nm)

Table 4: Observation space of Ant

Num	Observation	Min	Max	Name in XML	Joint	Unit
0/1/2	3-axis linear acceleration of the torso (including gravity)	-Inf	Inf	accelerometer	free	acceleration (m/s^2)
3/4/5	3-axis linear velocity of the torso	-Inf	Inf	velocimeter	free	velocity (m/s)
6/7/8	3-axis angular velocity velocity of the torso	-Inf	Inf	gyro	free	angular velocity (rad/s)
9/10/11	3D magnetic flux vector at the torso	-Inf	Inf	magnetometer	free	magnetic flux density (T)
12	Contact force at the front left ankle	0	Inf	touch_ankle_1a	-	force(N)
13	Contact force at the front right ankle	0	Inf	touch_ankle_2a	-	force(N)
14	Contact force at the back left ankle	0	Inf	touch_ankle_3a	-	force(N)
15	Contact force at the back left ankle	0	Inf	touch_ankle_4a	-	force(N)
16	Contact force at the end of the front left leg	0	Inf	touch_ankle_1b	-	force(N)
17	Contact force at the end of the front right leg	0	Inf	touch_ankle_2b	-	force(N)
18	Contact force at the end of the back left leg	0	Inf	touch_ankle_3b	-	force(N)
19	Contact force at the end of the back left leg	0	Inf	touch_ankle_4b	-	force(N)
20	Angle of the front left hip	-Inf	Inf	jointpos_hip_1	hinge	angle (rad)
21	Angle of the front right hip	-Inf	Inf	jointpos_hip_2	hinge	angle (rad)
22	Angle of the back left hip	-Inf	Inf	jointpos_hip_3	hinge	angle (rad)
23	Angle of the back right hip	-Inf	Inf	jointpos_hip_4	hinge	angle (rad)
24	Angle of the front left ankle	-Inf	Inf	jointpos_ankle_1	hinge	angle (rad)
25	Angle of the front right ankle	-Inf	Inf	jointpos_ankle_2	hinge	angle (rad)
26	Angle of the back left ankle	-Inf	Inf	jointpos_ankle_3	hinge	angle (rad)
27	Angle of the back right ankle	-Inf	Inf	jointpos_ankle_4	hinge	angle (rad)
28	Angular velocity of the front left hip	-Inf	Inf	jointvel_hip_1	hinge	angular velocity (rad/s)
29	Angular velocity of the front right hip	-Inf	Inf	jointvel_hip_2	hinge	angular velocity (rad/s)
30	Angular velocity of the back left hip	-Inf	Inf	jointvel_hip_3	hinge	angular velocity (rad/s)
31	Angular velocity of the back right hip	-Inf	Inf	jointvel_hip_4	hinge	angular velocity (rad/s)
32	Angular velocity of the front left ankle	-Inf	Inf	jointvel_ankle_1	hinge	angular velocity (rad/s)
33	Angular velocity of the front right ankle	-Inf	Inf	jointvel_ankle_2	hinge	angular velocity (rad/s)
34	Angular velocity of the back left ankle	-Inf	Inf	jointvel_ankle_3	hinge	angular velocity (rad/s)
35	Angular velocity of the back right ankle	-Inf	Inf	jointvel_ankle_4	hinge	angular velocity (rad/s)

Table 5: Action space of Walker

Num	Action	Min	Max	Name in XML	Joint	Unit
0	Torque applied on the rotor between torso and the right hip (x-coordinate)	-1	1	right_hip_x	hinge	torque (Nm)
1	Torque applied on the rotor between torso and the right hip (z-coordinate)	-1	1	right_hip_z	hinge	torque (Nm)
2	Torque applied on the rotor between torso and the right hip (y-coordinate)	-1	1	right_hip_y	hinge	torque (Nm)
3	Torque applied on the right leg rotor	-1	1	right_leg_joint	hinge	torque (Nm)
4	Torque applied on the right foot rotor	-1	1	right_foot_joint	hinge	torque (Nm)
5	Torque applied on the rotor between torso and the left hip (x-coordinate)	-1	1	left_hip_x	hinge	torque (Nm)
6	Torque applied on the rotor between torso and the left hip (z-coordinate)	-1	1	left_hip_z	hinge	torque (Nm)
7	Torque applied on the rotor between torso and the left hip (y-coordinate)	-1	1	left_hip_y	hinge	torque (Nm)
8	Torque applied on the left leg rotor	-1	1	left_leg_joint	hinge	torque (Nm)
9	Torque applied on the left foot rotor	-1	1	left_foot_joint	hinge	torque (Nm)

Table 6: Observation space of Walker

Num	Observation	Min	Max	Name in XML	Joint	Unit
0/1/2	3-axis linear acceleration of the torso (including gravity)	-Inf	Inf	accelerometer	free	acceleration (m/s^2)
3/4/5	3-axis linear velocity of the torso	-Inf	Inf	velocimeter	free	velocity (m/s)
6/7/8	3-axis angular velocity velocity of the torso	-Inf	Inf	gyro	free	angular velocity (rad/s)
9/10/11	3D magnetic flux vector at the torso	-Inf	Inf	magnetometer	free	magnetic flux density (T)
12	Contact force at the right foot	0	Inf	touch_right_foot	-	force(N)
13	Contact force at the left foot	0	Inf	touch_left_foot	-	force(N)
14	Angle of the right hip (x-coordinate)	-Inf	Inf	jointpos_right_hip_x	hinge	angle (rad)
15	Angle of the right hip (z-coordinate)	-Inf	Inf	jointpos_right_hip_z	hinge	angle (rad)
16	Angle of the right hip (y-coordinate)	-Inf	Inf	jointpos_right_hip_y	hinge	angle (rad)
17	Angle of the right leg	-Inf	Inf	jointpos_right_leg	hinge	angle (rad)
18	Angle of the right foot	-Inf	Inf	jointpos_right_foot	hinge	angle (rad)
19	Angle of the left hip (x-coordinate)	-Inf	Inf	jointpos_left_hip_x	hinge	angle (rad)
20	Angle of the left hip (z-coordinate)	-Inf	Inf	jointpos_left_hip_z	hinge	angle (rad)
21	Angle of the left hip (y-coordinate)	-Inf	Inf	jointpos_left_hip_y	hinge	angle (rad)
22	Angle of the left leg	-Inf	Inf	jointpos_left_leg	hinge	angle (rad)
23	Angle of the left foot	-Inf	Inf	jointpos_left_foot	hinge	angle (rad)
24	Angular velocity of the right hip (x-coordinate)	-Inf	Inf	jointvel_right_hip_x	hinge	angular velocity (rad/s)
25	Angular velocity of the right hip (z-coordinate)	-Inf	Inf	jointvel_right_hip_z	hinge	angular velocity (rad/s)
26	Angular velocity of the right hip (y-coordinate)	-Inf	Inf	jointvel_right_hip_y	hinge	angular velocity (rad/s)
27	Angular velocity of the right leg	-Inf	Inf	jointvel_right_leg	hinge	angular velocity (rad/s)
28	Angular velocity of the right foot	-Inf	Inf	jointvel_right_foot	hinge	angular velocity (rad/s)
29	Angular velocity of the left hip (x-coordinate)	-Inf	Inf	jointvel_left_hip_x	hinge	angular velocity (rad/s)
30	Angular velocity of the left hip (z-coordinate)	-Inf	Inf	jointvel_left_hip_z	hinge	angular velocity (rad/s)
31	Angular velocity of the left hip (y-coordinate)	-Inf	Inf	jointvel_left_hip_y	hinge	angular velocity (rad/s)
32	Angular velocity of the left leg	-Inf	Inf	jointvel_left_leg	hinge	angular velocity (rad/s)
33	Angular velocity of the left foot	-Inf	Inf	jointvel_left_foot	hinge	angular velocity (rad/s)

Table 7: Action space of Humanoid

Num	Action	Min	Max	Name in XML	Joint	Unit
0	Torque applied on the rotor between torso and the right hip (x-coordinate)	-1	1	right_hip_x	hinge	torque (Nm)
1	Torque applied on the rotor between torso and the right hip (z-coordinate)	-1	1	right_hip_z	hinge	torque (Nm)
2	Torque applied on the rotor between torso and the right hip (y-coordinate)	-1	1	right_hip_y	hinge	torque (Nm)
3	Torque applied on the right knee rotor	-1	1	right_knee	hinge	torque (Nm)
4	Torque applied on the rotor between torso and the left hip (x-coordinate)	-1	1	left_hip_x	hinge	torque (Nm)
5	Torque applied on the rotor between torso and the left hip (z-coordinate)	-1	1	left_hip_z	hinge	torque (Nm)
6	Torque applied on the rotor between torso and the left hip (y-coordinate)	-1	1	left_hip_y	hinge	torque (Nm)
7	Torque applied on the left knee rotor	-1	1	left_knee	hinge	torque (Nm)

Table 8: Observation space of Humanoid

Num	Observation	Min	Max	Name in XML	Joint	Unit
0/1/2	3-axis linear acceleration of the torso (including gravity)	-Inf	Inf	accelerometer	free	acceleration (m/s^2)
3/4/5	3-axis linear velocity of the torso	-Inf	Inf	velocimeter	free	velocity (m/s)
6/7/8	3-axis angular velocity velocity of the torso	-Inf	Inf	gyro	free	angular velocity (rad/s)
9/10/11	3D magnetic flux vector at the torso	-Inf	Inf	magnetometer	free	magnetic flux density (T)
12	Contact force at the right foot	0	Inf	touch_right_foot	-	force(N)
13	Contact force at the left foot	0	Inf	touch_left_foot	-	force(N)
14	Angle of the right hip (x-coordinate)	-Inf	Inf	jointpos_right_hip_x	hinge	angle (rad)
15	Angle of the right hip (z-coordinate)	-Inf	Inf	jointpos_right_hip_z	hinge	angle (rad)
16	Angle of the right hip (y-coordinate)	-Inf	Inf	jointpos_right_hip_y	hinge	angle (rad)
17	Angle of the right knee	-Inf	Inf	jointpos_right_knee	hinge	angle (rad)
18	Angle of the left hip (x-coordinate)	-Inf	Inf	jointpos_left_hip_x	hinge	angle (rad)
19	Angle of the left hip (z-coordinate)	-Inf	Inf	jointpos_left_hip_z	hinge	angle (rad)
20	Angle of the left hip (y-coordinate)	-Inf	Inf	jointpos_left_hip_y	hinge	angle (rad)
21	Angle of the left leg	-Inf	Inf	jointpos_left_knee	hinge	angle (rad)
22	Angular velocity of the right hip (x-coordinate)	-Inf	Inf	jointvel_right_hip_x	hinge	angular velocity (rad/s)
23	Angular velocity of the right hip (z-coordinate)	-Inf	Inf	jointvel_right_hip_z	hinge	angular velocity (rad/s)
24	Angular velocity of the right hip (y-coordinate)	-Inf	Inf	jointvel_right_hip_y	hinge	angular velocity (rad/s)
25	Angular velocity of the right knee	-Inf	Inf	jointvel_right_knee	hinge	angular velocity (rad/s)
26	Angular velocity of the left hip (x-coordinate)	-Inf	Inf	jointvel_left_hip_x	hinge	angular velocity (rad/s)
27	Angular velocity of the left hip (z-coordinate)	-Inf	Inf	jointvel_left_hip_z	hinge	angular velocity (rad/s)
28	Angular velocity of the left hip (y-coordinate)	-Inf	Inf	jointvel_left_hip_y	hinge	angular velocity (rad/s)
29	Angular velocity of the left knee	-Inf	Inf	jointvel_left_knee	hinge	angular velocity (rad/s)

Table 9: Action space of Hopper

Num	Action	Min	Max	Name in XML	Joint	Unit
0	Torque applied on the rotor between torso and the hip (x-coordinate)	-1	1	hip_x	hinge	torque (Nm)
1	Torque applied on the rotor between torso and the hip (z-coordinate)	-1	1	hip_z	hinge	torque (Nm)
2	Torque applied on the rotor between torso and the hip (y-coordinate)	-1	1	hip_y	hinge	torque (Nm)
3	Torque applied on the thigh rotor	-1	1	thigh_joint	hinge	torque (Nm)
4	Torque applied on the leg rotor	-1	1	leg_joint	hinge	torque (Nm)
5	Torque applied on the foot rotor	-1	1	foot_joint	hinge	torque (Nm)

Table 10: Observation space of Hopper

Num	Observation	Min	Max	Name in XML	Joint	Unit
0/1/2	3-axis linear acceleration of the torso (including gravity)	-Inf	Inf	accelerometer	free	acceleration (m/s^2)
3/4/5	3-axis linear velocity of the torso	-Inf	Inf	velocimeter	free	velocity (m/s)
6/7/8	3-axis angular velocity velocity of the torso	-Inf	Inf	gyro	free	angular velocity (rad/s)
9/10/11	3D magnetic flux vector at the torso	-Inf	Inf	magnetometer	free	magnetic flux density (T)
12	Contact force at the foot	0	Inf	touch_foot	-	force(N)
13	Angle of the hip (x-coordinate)	-Inf	Inf	jointpos_hip_x	hinge	angle (rad)
14	Angle of the hip (z-coordinate)	-Inf	Inf	jointpos_hip_z	hinge	angle (rad)
15	Angle of the hip (y-coordinate)	-Inf	Inf	jointpos_hip_y	hinge	angle (rad)
16	Angle of the thigh	-Inf	Inf	jointpos_thigh	hinge	angle (rad)
17	Angle of the leg	-Inf	Inf	jointpos_leg	hinge	angle (rad)
18	Angle of the foot	-Inf	Inf	jointpos_foot	hinge	angle (rad)
19	Angular velocity of the hip (x-coordinate)	-Inf	Inf	jointvel_hip_x	hinge	angular velocity (rad/s)
20	Angular velocity of the hip (z-coordinate)	-Inf	Inf	jointvel_hip_z	hinge	angular velocity (rad/s)
21	Angular velocity of the hip (y-coordinate)	-Inf	Inf	jointvel_hip_y	hinge	angular velocity (rad/s)
22	Angular velocity of the thigh	-Inf	Inf	jointvel_thigh	hinge	angular velocity (rad/s)
23	Angular velocity of the leg	-Inf	Inf	jointvel_leg	hinge	angular velocity (rad/s)
24	Angular velocity of the foot	-Inf	Inf	jointvel_foot	hinge	angular velocity (rad/s)

Table 11: Action space of Arm3

Num	Action	Min	Max	Name in XML	Joint	Unit
0	Torque applied on the first joint (connecting the base point and the first link)	-1	1	joint_1	hinge	torque (Nm)
1	Torque applied on the second joint(connecting the first and the second link)	-1	1	joint_2	hinge	torque (Nm)
2	Torque applied on the third joint (connecting the second and the third link)	-1	1	joint_3	hinge	torque (Nm)

Table 12: Observation space of Arm3

Num	Observation	Min	Max	Name in XML	Joint	Unit
0/1/2	3-axis linear acceleration of the first link (including gravity)	-Inf	Inf	accelerometer_link_1	free	acceleration (m/s^2)
3/4/5	3-axis linear velocity of the first link	-Inf	Inf	velocimeter_link_1	free	velocity (m/s)
6/7/8	3-axis angular velocity velocity of the first link	-Inf	Inf	gyro_link_1	free	angular velocity (rad/s)
9/10/11	3D magnetic flux vector at the first link	-Inf	Inf	magnetometer_link_1	free	magnetic flux density (T)
12/13/14	3-axis linear acceleration of the second link (including gravity)	-Inf	Inf	accelerometer_link_2	free	acceleration (m/s^2)
15/16/17	3-axis linear velocity of the second link	-Inf	Inf	velocimeter_link_2	free	velocity (m/s)
18/19/20	3-axis angular velocity velocity of the second link	-Inf	Inf	gyro_link_2	free	angular velocity (rad/s)
21/22/23	3D magnetic flux vector at the second link	-Inf	Inf	magnetometer_link_2	free	magnetic flux density (T)
24/25/26	3-axis linear acceleration of the third link (including gravity)	-Inf	Inf	accelerometer_link_3	free	acceleration (m/s^2)
27/28/29	3-axis linear velocity of the third link	-Inf	Inf	velocimeter_link_3	free	velocity (m/s)
30/31/32	3-axis angular velocity velocity of the third link	-Inf	Inf	gyro_link_3	free	angular velocity (rad/s)
33/34/35	3D magnetic flux vector at the third link	-Inf	Inf	magnetometer_link_3	free	magnetic flux density (T)
36/37/38	3-axis linear acceleration of the fourth link (including gravity)	-Inf	Inf	accelerometer_link_4	free	acceleration (m/s^2)
39/40/41	3-axis linear velocity of the fourth link	-Inf	Inf	velocimeter_link_4	free	velocity (m/s)
42/43/44	3-axis angular velocity velocity of the fourth link	-Inf	Inf	gyro_link_4	free	angular velocity (rad/s)
45/46/47	3D magnetic flux vector at the fourth link	-Inf	Inf	magnetometer_link_4	free	magnetic flux density (T)
48/49/50	3-axis linear acceleration of the fifth link (including gravity)	-Inf	Inf	accelerometer_link_5	free	acceleration (m/s^2)
51/52/53	3-axis linear velocity of the fifth link	-Inf	Inf	velocimeter_link_5	free	velocity (m/s)
54/55/56	3-axis angular velocity velocity of the fifth link	-Inf	Inf	gyro_link_5	free	angular velocity (rad/s)
57/58/59	3D magnetic flux vector at the fifth link	-Inf	Inf	magnetometer_link_5	free	magnetic flux density (T)
60	Angle of the first joint	-Inf	Inf	jointpos_joint_1	hinge	angle (rad)
61	Angle of the second joint	-Inf	Inf	jointpos_joint_2	hinge	angle (rad)
62	Angle of the third joint	-Inf	Inf	jointpos_joint_3	hinge	angle (rad)
63	Angular velocity of the first joint	-Inf	Inf	jointvel_joint_1	hinge	angular velocity (rad/s)
64	Angular velocity of the second joint	-Inf	Inf	jointvel_joint_2	hinge	angular velocity (rad/s)
65	Angular velocity of the third joint	-Inf	Inf	jointvel_joint_3	hinge	angular velocity (rad/s)
66	Contact force at the end effector	0	Inf	touch_end_effector	-	force(N)

Table 13: Action space of Arm6

Num	Action	Min	Max	Name in XML	Joint	Unit
0	Torque applied on the first joint (connecting the base point and the first link)	-1	1	joint_1	hinge	torque (Nm)
1	Torque applied on the second joint(connecting the first and the second link)	-1	1	joint_2	hinge	torque (Nm)
2	Torque applied on the third joint (connecting the second and the third link)	-1	1	joint_3	hinge	torque (Nm)
3	Torque applied on the fourth joint (connecting the third and the fourth link)	-1	1	joint_4	hinge	torque (Nm)
4	Torque applied on the fifth joint (connecting the fourth and the fifth link)	-1	1	joint_5	hinge	torque (Nm)
5	Torque applied on the sixth joint (connecting the fifth and the sixth link)	-1	1	joint_6	hinge	torque (Nm)

Table 14: Observation space of Arm6

Num	Observation	Min	Max	Name in XML	Joint	Unit
0/1/2	3-axis linear acceleration of the first link (including gravity)	-Inf	Inf	accelerometer_link_1	free	acceleration (m/s^2)
3/4/5	3-axis linear velocity of the first link	-Inf	Inf	velocimeter_link_1	free	velocity (m/s)
6/7/8	3-axis angular velocity velocity of the first link	-Inf	Inf	gyro_link_1	free	angular velocity (rad/s)
9/10/11	3D magnetic flux vector at the first link	-Inf	Inf	magnetometer_link_1	free	magnetic flux density (T)
12/13/14	3-axis linear acceleration of the second link (including gravity)	-Inf	Inf	accelerometer_link_2	free	acceleration (m/s^2)
15/16/17	3-axis linear velocity of the second link	-Inf	Inf	velocimeter_link_2	free	velocity (m/s)
18/19/20	3-axis angular velocity velocity of the second link	-Inf	Inf	gyro_link_2	free	angular velocity (rad/s)
21/22/23	3D magnetic flux vector at the second link	-Inf	Inf	magnetometer_link_2	free	magnetic flux density (T)
24/25/26	3-axis linear acceleration of the third link (including gravity)	-Inf	Inf	accelerometer_link_3	free	acceleration (m/s^2)
27/28/29	3-axis linear velocity of the third link	-Inf	Inf	velocimeter_link_3	free	velocity (m/s)
30/31/32	3-axis angular velocity velocity of the third link	-Inf	Inf	gyro_link_3	free	angular velocity (rad/s)
33/34/35	3D magnetic flux vector at the third link	-Inf	Inf	magnetometer_link_3	free	magnetic flux density (T)
36/37/38	3-axis linear acceleration of the fourth link (including gravity)	-Inf	Inf	accelerometer_link_4	free	acceleration (m/s^2)
39/40/41	3-axis linear velocity of the fourth link	-Inf	Inf	velocimeter_link_4	free	velocity (m/s)
42/43/44	3-axis angular velocity velocity of the fourth link	-Inf	Inf	gyro_link_4	free	angular velocity (rad/s)
45/46/47	3D magnetic flux vector at the fourth link	-Inf	Inf	magnetometer_link_4	free	magnetic flux density (T)
48/49/50	3-axis linear acceleration of the fifth link (including gravity)	-Inf	Inf	accelerometer_link_5	free	acceleration (m/s^2)
51/52/53	3-axis linear velocity of the fifth link	-Inf	Inf	velocimeter_link_5	free	velocity (m/s)
54/55/56	3-axis angular velocity velocity of the fifth link	-Inf	Inf	gyro_link_5	free	angular velocity (rad/s)
57/58/59	3D magnetic flux vector at the fifth link	-Inf	Inf	magnetometer_link_5	free	magnetic flux density (T)
60/61/62	3-axis linear acceleration of the sixth link (including gravity)	-Inf	Inf	accelerometer_link_6	free	acceleration (m/s^2)
63/64/65	3-axis linear velocity of the sixth link	-Inf	Inf	velocimeter_link_6	free	velocity (m/s)
66/67/68	3-axis angular velocity velocity of the sixth link	-Inf	Inf	gyro_link_6	free	angular velocity (rad/s)
69/70/71	3D magnetic flux vector at the sixth link	-Inf	Inf	magnetometer_link_6	free	magnetic flux density (T)
72/73/74	3-axis linear acceleration of the seventh link (including gravity)	-Inf	Inf	accelerometer_link_7	free	acceleration (m/s^2)
75/76/77	3-axis linear velocity of the seventh link	-Inf	Inf	velocimeter_link_7	free	velocity (m/s)
78/79/80	3-axis angular velocity velocity of the seventh link	-Inf	Inf	gyro_link_7	free	angular velocity (rad/s)
81/82/83	3D magnetic flux vector at the seventh link	-Inf	Inf	magnetometer_link_7	free	magnetic flux density (T)
84	Angle of the first joint	-Inf	Inf	jointpos_joint_1	hinge	angle (rad)
85	Angle of the second joint	-Inf	Inf	jointpos_joint_2	hinge	angle (rad)
86	Angle of the third joint	-Inf	Inf	jointpos_joint_3	hinge	angle (rad)
87	Angle of the fourth joint	-Inf	Inf	jointpos_joint_4	hinge	angle (rad)
88	Angle of the fifth joint	-Inf	Inf	jointpos_joint_5	hinge	angle (rad)
89	Angle of the sixth joint	-Inf	Inf	jointpos_joint_6	hinge	angle (rad)
90	Angular velocity of the first joint	-Inf	Inf	jointvel_joint_1	hinge	angular velocity (rad/s)
91	Angular velocity of the second joint	-Inf	Inf	jointvel_joint_2	hinge	angular velocity (rad/s)
92	Angular velocity of the third joint	-Inf	Inf	jointvel_joint_3	hinge	angular velocity (rad/s)
93	Angular velocity of the fourth joint	-Inf	Inf	jointvel_joint_4	hinge	angular velocity (rad/s)
94	Angular velocity of the fifth joint	-Inf	Inf	jointvel_joint_5	hinge	angular velocity (rad/s)
95	Angular velocity of the sixth joint	-Inf	Inf	jointvel_joint_6	hinge	angular velocity (rad/s)
96	Contact force at the end effector	0	Inf	touch_end_effector	-	force(N)

Table 15: Action space of Drone

Num	Action	Min	Max	Name in XML	Joint	Unit
0	Extra thrust force applied on the first propeller	-1	1	-	-	force (N)
1	Extra thrust force applied on the second propeller	-1	1	-	-	force (N)
2	Extra thrust force applied on the third propeller	-1	1	-	-	force (N)
3	Extra thrust force applied on the fourth propeller	-1	1	-	-	force (N)

Table 16: Observation space of Drone

Num	Observation	Min	Max	Name in XML	Joint	Unit
0/1/2	3-axis linear acceleration of the torso (including gravity)	-Inf	Inf	accelerometer	free	acceleration (m/s^2)
3/4/5	3-axis linear velocity of the torso	-Inf	Inf	velocimeter	free	velocity (m/s)
6/7/8	3-axis angular velocity velocity of the torso	-Inf	Inf	gyro	free	angular velocity (rad/s)
9/10/11	3D magnetic flux vector at the torso	-Inf	Inf	magnetometer	free	magnetic flux density (T)
12	Contact force at the upper point of the first propeller	0	Inf	touch_p1a	-	force(N)
13	Contact force at the lower point of the first propeller	0	Inf	touch_p1b	-	force(N)
14	Contact force at the upper point of the second propeller	0	Inf	touch_p2a	-	force(N)
15	Contact force at the lower point of the second propeller	0	Inf	touch_p2b	-	force(N)
16	Contact force at the upper point of the third propeller	0	Inf	touch_p3a	-	force(N)
17	Contact force at the lower point of the third propeller	0	Inf	touch_p3b	-	force(N)
18	Contact force at the upper point of the fourth propeller	0	Inf	touch_p4a	-	force(N)
19	Contact force at the lower point of the fourth propeller	0	Inf	touch_p4b	-	force(N)

B.2 Observation Space Options and Desiderata

The observation spaces are also updated to match the new 3D tasks. The 3D compasses and 3D pseudo-lidars are introduced for 3D robots to sensor the position of targets in 3D space. Different from the single lidar system of the original environmet, the Advanced Safety Gym allows to apply multiple lidars on different parts of the robot. For example, in Figure 12a the Arm robot is equipped with a 3D lidar and a 3D compass on each joint to obtain more environment information. Figure 12b shows a drone equipped with two 3D lidars to observe the 3D hazards and the 3D goal. The "lidar halos" of two lidars are distributed on two sphere with different radius. The number of "lidar halos" is configurable for more dense observations.

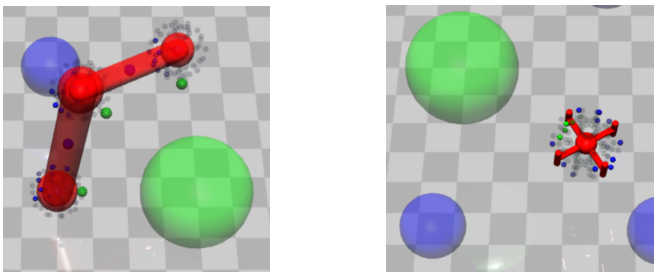

(a) (b)

Figure 12: Visualizations of observation spaces

B.3 Layout Randomization Options and Desiderata

The layout randomization is inherited from the original Safety Gym. In order to generate 3D objects, the z coordinate can be configured or randomly picked after the x and y coordinates are generated.

B.4 Task and Constraint Details

Table 17: Comparison between different tasks

	GUARD Tasks				SafetyGym Tasks		
	Goal	Push	Chase	Defense	Goal	Button	Push
Interactive task		✓	✓	✓			✓
Non-interactive task	✓				✓	✓	
Contact task		✓	✓	✓		✓	✓
Non-contact task	✓		✓	✓	✓		
2D task	✓	✓	✓	✓	✓	✓	✓
3D task	✓		✓	✓			
Movable target		✓	✓	✓			✓
Immovable target	✓				✓	✓	
Single target	✓	✓	✓	✓	✓	✓	✓
Multiple targets			✓	✓			
General contact target		✓	✓	✓		✓	

Table 18: Comparison between different constraints

	New Constraints			Inherited Constraints				
	Ghosts	Ghosts 3D	Hazards 3D	Hazards	Vases	Pillars	Buttons	Gremlins
Trespassable	✓	✓			✓	✓	✓	✓
Untrespassable	✓	✓	✓	✓				
Immovable			✓	✓		✓	✓	
Passively movable					✓			
Actively movable	✓	✓						✓
3D motion		✓	✓					
2D motion	✓	✓	✓	✓	✓	✓	✓	✓

B.5 Dynamics of movable objects

We begin by defining the distance vector $d_{\text{origin}} = x_{\text{origin}} - x_{\text{object}}$, which represents the distance from the position of the dynamic object x_{object} to the origin point of the world framework x_{origin}. By default, the origin point is set to $(0, 0, 0)$. Next, we define the distance vector $d_{\text{robot}} = x_{\text{robot}} - x_{\text{object}}$, which represents the distance from the dynamic object x_{object} to the position of the robot x_{robot}. We introduce two parameters: r_0, which defines a circular area centered at the origin point within which the objects are limited to move. r_1, which represents the threshold distance that the dynamic objects strive to maintain from the robot. Finally, we have three configurable non-negative velocity constants for the dynamic objects: v_0, v_1, and v_2.

B.5.1 Dynamics of targets of Chase task

$$\dot{x}_{object} = \begin{cases} v_0 * d_{origin}, & \text{if } \|d_{origin}\| > r_0 \\ -v_1 * d_{robot}, & \text{if } \|d_{origin}\| \leq r_0 \text{ and } \|d_{robot}\| \leq r_1 \\ 0, & \text{if } \|d_{origin}\| \leq r_0 \text{ and } \|d_{robot}\| > r_1 \end{cases}, \tag{11}$$

B.5.2 Dynamics of targets of Defense task

$$\dot{x}_{object} = \begin{cases} v_0 * d_{origin}, & \text{if } \|d_{origin}\| > r_0 \\ -v_1 * d_{robot}, & \text{if } \|d_{origin}\| \leq r_0 \text{ and } \|d_{robot}\| \leq r_1 \\ v_2 * d_{origin}, & \text{if } \|d_{origin}\| \leq r_0 \text{ and } \|d_{robot}\| > r_1 \end{cases}, \tag{12}$$

B.5.3 Dynamics of ghost and 3D ghost

$$\dot{x}_{object} = \begin{cases} v_0 * d_{origin}, & \text{if } \|d_{origin}\| > r_0 \\ v_1 * d_{robot}, & \text{if } \|d_{origin}\| \leq r_0 \text{ and } \|d_{robot}\| > r_1 \\ 0, & \text{if } \|d_{origin}\| \leq r_0 \text{ and } \|d_{robot}\| \leq r_1 \end{cases}, \tag{13}$$

C Expeiment Details

The GUARD implementation is partially inspired by Safety Gym (Ray et al., 2019) and Spinningup (Achiam, 2018) which are both under MIT license.

C.1 Policy Settings

The hyper-parameters used in our experiments are listed in Table 19 as default.

Our experiments use separate multi-layer perception with *tanh* activations for the policy network, value network and cost network. Each network consists of two hidden layers of size (64,64). All of the networks are trained using *Adam* optimizer with learning rate of 0.01.

We apply an on-policy framework in our experiments. During each epoch the agent interact B times with the environment and then perform a policy update based on the experience collected from the current epoch. The maximum length of the trajectory is set to 1000 and the total epoch number N is set to 200 as default. In our experiments the Walker and the Ant were trained for 1000 epochs due to the high dimension.

The policy update step is based on the scheme of TRPO, which performs up to 100 steps of backtracking with a coefficient of 0.8 for line searching.

For all experiments, we use a discount factor of $\gamma = 0.99$, an advantage discount factor $\lambda = 0.95$, and a KL-divergence step size of $\delta_{KL} = 0.02$.

For experiments which consider cost constraints we adopt a target cost $\delta_c = 0.0$ to pursue a zero-violation policy.

Other unique hyper-parameters for each algorithms are hand-tuned to attain reasonable performance.

Each model is trained on a server with a 48-core Intel(R) Xeon(R) Silver 4214 CPU @ 2.2.GHz, Nvidia RTX A4000 GPU with 16GB memory, and Ubuntu 20.04.

For low-dimensional tasks, we train each model for 6e6 steps which takes around seven hours. For high-dimensional tasks, we train each model for 3e7 steps which takes around 60 hours.

C.2 Experiment tasks

The experiment settings, detailed in Table 20, encompass a total of 72 combinations derived from 4 task types, 9 robot types, and 2 constraint types. For the purpose of comprehensive comparison in this paper, we have selected 36 experiments involving 8 hazards and 9 experiments featuring 8 ghosts.

C.3 Metrics Comparison

we report all the 45 results of our test suites by three metrics:

- The average episode return J_r.
- The average episodic sum of costs M_c.
- The average cost over the entirety of training ρ_c.

All of the three metrics were obtained from the final epoch after convergence. Each metric was averaged over two random seed.

Table 19: Important hyper-parameters of different algorithms in our experiments

Policy Parameter		TRPO	TRPO-Lagrangian	TRPO-SL [18' Dalal]	TRPO-USL	TRPO-IPO	TRPO-FAC	CPO	PCPO
Epochs	N	200	200	200	200	200	200	200	200
Steps per epoch	B	30000	30000	30000	30000	30000	30000	30000	30000
Maximum length of trajectory	L	1000	1000	1000	1000	1000	1000	1000	1000
Policy network hidden layers		(64, 64)	(64, 64)	(64, 64)	(64, 64)	(64, 64)	(64, 64)	(64, 64)	(64, 64)
Discount factor	γ	0.99	0.99	0.99	0.99	0.99	0.99	0.99	0.99
Advantage discount factor	λ	0.97	0.97	0.97	0.97	0.97	0.97	0.97	0.97
TRPO backtracking steps		100	100	100	100	100	100	100	-
TRPO backtracking coefficient		0.8	0.8	0.8	0.8	0.8	0.8	0.8	-
Target KL	δ_{KL}	0.02	0.02	0.02	0.02	0.02	0.02	0.02	0.02
Value network hidden layers		(64, 64)	(64, 64)	(64, 64)	(64, 64)	(64, 64)	(64, 64)	(64, 64)	(64, 64)
Value network iteration		80	80	80	80	80	80	80	80
Value network optimizer		Adam	Adam	Adam	Adam	Adam	Adam	Adam	Adam
Value learning rate		0.001	0.001	0.001	0.001	0.001	0.001	0.001	0.001
Cost network hidden layers		-	(64, 64)	(64, 64)	(64, 64)	-	(64, 64)	(64, 64)	(64, 64)
Cost network iteration		-	80	80	80	-	80	80	80
Cost network optimizer		-	Adam	Adam	Adam	-	Adam	Adam	Adam
Cost learning rate		-	0.001	0.001	0.001	-	0.001	0.001	0.001
Target Cost	δ_c	-	0.0	0.0	0.0	0.0	0.0	0.0	0.0
Lagrangian optimizer		-	-	-	-	-	Adam	-	-
Lagrangian learning rate		-	0.005	-	-	-	0.0001	-	-
USL correction iteration		-	-	-	20	-	-	-	-
USL correction rate		-	-	-	0.05	-	-	-	-
Warmup ratio		-	-	1/3	1/3	-	-	-	-
IPO parameter	t	-	-	-	-	0.01	-	-	-
Cost reduction		-	-	-	-	-	-	0.0	-

Goal_Point_8Hazards
Goal_Point_8Ghosts
Goal_Swimmer_8Hazards
Goal_Swimmer_8Ghosts
Goal_Ant_8Hazards
Goal_Ant_8Ghosts
Goal_Walker_8Hazards
Goal_Walker_8Ghosts
Goal_Humanoid_8Hazards
Goal_Humanoid_8Ghosts
Goal_Hopper_8Hazards
Goal_Hopper_8Ghosts
Goal_Arm3_8Hazards
Goal_Arm3_8Ghosts
Goal_Arm6_8Hazards
Goal_Arm6_8Ghosts
Goal_Drone_8Hazards
Goal_Drone_8Ghosts

(a) Goal

Push_Point_8Hazards
Push_Point_8Ghosts
Push_Swimmer_8Hazards
Push_Swimmer_8Ghosts
Push_Ant_8Hazards
Push_Ant_8Ghosts
Push_Walker_8Hazards
Push_Walker_8Ghosts
Push_Humanoid_8Hazards
Push_Humanoid_8Ghosts
Push_Hopper_8Hazards
Push_Hopper_8Ghosts
Push_Arm3_8Hazards
Push_Arm3_8Ghosts
Push_Arm6_8Hazards
Push_Arm6_8Ghosts
Push_Drone_8Hazards
Push_Drone_8Ghosts

(b) Push

Chase_Point_8Hazards
Chase_Point_8Ghosts
Chase_Swimmer_8Hazards
Chase_Swimmer_8Ghosts
Chase_Ant_8Hazards
Chase_Ant_8Ghosts
Chase_Walker_8Hazards
Chase_Walker_8Ghosts
Chase_Humanoid_8Hazards
Chase_Humanoid_8Ghosts
Chase_Hopper_8Hazards
Chase_Hopper_8Ghosts
Chase_Arm3_8Hazards
Chase_Arm3_8Ghosts
Chase_Arm6_8Hazards
Chase_Arm6_8Ghosts
Chase_Drone_8Hazards
Chase_Drone_8Ghosts

(c) Chase

Defense_Point_8Hazards
Defense_Point_8Ghosts
Defense_Swimmer_8Hazards
Defense_Swimmer_8Ghosts
Defense_Ant_8Hazards
Defense_Ant_8Ghosts
Defense_Walker_8Hazards
Defense_Walker_8Ghosts
Defense_Humanoid_8Hazards
Defense_Humanoid_8Ghosts
Defense_Hopper_8Hazards
Defense_Hopper_8Ghosts
Defense_Arm3_8Hazards
Defense_Arm3_8Ghosts
Defense_Arm6_8Hazards
Defense_Arm6_8Ghosts
Defense_Drone_8Hazards
Defense_Drone_8Ghosts

(d) Defense

Table 20: Tasks of our environments

Table 21: Metrics of nine **Goal_{Robot}_8Hazards** environments obtained from the final epoch.

Goal_Point_8Hazards

Algorithm	$\bar{J}_r$	$\bar{M}_c$	$\bar{\rho}_c$
TRPO	26.2296	7.4550	0.0067
TRPO-Lagrangian	25.4503	2.5031	**0.0034**
TRPO-SL	19.0765	3.5200	0.0056
TRPO-USL	24.6524	7.0004	0.0060
TRPO-IPO	20.3057	4.4037	0.0049
TRPO-FAC	**26.9707**	**2.1581**	0.0038
CPO	25.9157	3.2388	0.0036
PCPO	24.9032	3.7118	0.0048

Goal_Swimmer_8Hazards

Algorithm	$\bar{J}_r$	$\bar{M}_c$	$\bar{\rho}_c$
TRPO	**31.5282**	11.4067	0.0117
TRPO-Lagrangian	19.5685	**4.3231**	**0.0074**
TRPO-SL	9.2362	4.4453	0.0075
TRPO-USL	30.2756	10.2352	0.0100
TRPO-IPO	9.5714	7.9993	0.0079
TRPO-FAC	24.8486	7.8014	0.0085
CPO	26.6166	9.2452	0.0095
PCPO	24.4054	9.3452	0.0094

Goal_Ant_8Hazards

Algorithm	$\bar{J}_r$	$\bar{M}_c$	$\bar{\rho}_c$
TRPO	59.3694	7.9737	0.0097
TRPO-Lagrangian	35.0180	**2.7954**	**0.0056**
TRPO-SL	24.0752	45.9755	0.0355
TRPO-USL	59.2213	9.2237	0.0096
TRPO-IPO	2.6040	6.3006	0.0059
TRPO-FAC	48.2685	5.6736	0.0071
CPO	60.2093	8.1194	0.0092
PCPO	**60.3654**	8.9137	0.0091

Goal_Walker_8Hazards

Algorithm	$\bar{J}_r$	$\bar{M}_c$	$\bar{\rho}_c$
TRPO	56.7139	9.8112	0.0104
TRPO-Lagrangian	33.7839	**3.3714**	**0.0053**
TRPO-SL	39.9848	12.7370	0.0128
TRPO-USL	**57.1097**	9.9469	0.0097
TRPO-IPO	7.2728	6.7115	0.0068
TRPO-FAC	42.6250	4.4426	0.0062
CPO	51.9246	8.0409	0.0082
PCPO	55.0100	10.0377	0.0089

Goal_Humanoid_8Hazards

Algorithm	$\bar{J}_r$	$\bar{M}_c$	$\bar{\rho}_c$
TRPO	11.6758	8.2332	0.0079
TRPO-Lagrangian	6.1294	7.6847	**0.0066**
TRPO-SL	9.1517	10.1473	0.0091
TRPO-USL	10.9310	9.2950	0.0079
TRPO-IPO	2.5561	9.0792	0.0071
TRPO-FAC	10.0730	8.3481	0.0068
CPO	**11.9573**	**6.0618**	0.0074
PCPO	11.6731	6.8256	0.0074

Goal_Hopper_8Hazards

Algorithm	$\bar{J}_r$	$\bar{M}_c$	$\bar{\rho}_c$
TRPO	**32.8406**	7.3477	0.0082
TRPO-Lagrangian	24.2180	6.4342	**0.0069**
TRPO-SL	26.1236	8.9366	0.0098
TRPO-USL	32.5692	8.1526	0.0080
TRPO-IPO	4.0118	7.2667	0.0082
TRPO-FAC	28.1388	**6.3430**	0.0076
CPO	27.2544	8.0783	0.0076
PCPO	30.7637	6.4343	0.0076

Goal_Arm3_8Hazards

Algorithm	$\bar{J}_r$	$\bar{M}_c$	$\bar{\rho}_c$
TRPO	19.8716	23.8574	0.0293
TRPO-Lagrangian	6.0512	2.1411	**0.0057**
TRPO-SL	4.2161	**0.4820**	0.0115
TRPO-USL	15.6522	8.6754	0.0163
TRPO-IPO	2.4211	12.5567	0.0199
TRPO-FAC	10.0948	3.3072	0.0085
CPO	16.2682	22.1031	0.0210
PCPO	**21.5110**	16.2963	0.0211

Goal_Arm6_8Hazards

Algorithm	$\bar{J}_r$	$\bar{M}_c$	$\bar{\rho}_c$
TRPO	4.3703	15.0087	0.0206
TRPO-Lagrangian	1.2386	6.8767	**0.0107**
TRPO-SL	2.1136	14.1806	0.0136
TRPO-USL	2.5704	9.4493	0.0186
TRPO-IPO	0.8242	**5.5569**	0.0129
TRPO-FAC	2.4243	8.9828	0.0124
CPO	**4.3885**	13.0115	0.0171
PCPO	1.1528	13.8961	0.0141

Goal_Drone_8Hazards

Algorithm	$\bar{J}_r$	$\bar{M}_c$	$\bar{\rho}_c$
TRPO	**19.6492**	1.6839	0.0012
TRPO-Lagrangian	17.5182	1.0479	0.0010
TRPO-SL	11.0012	**0.2030**	0.0004
TRPO-USL	17.3535	1.1217	0.0008
TRPO-IPO	15.7189	0.8852	0.0007
TRPO-FAC	17.0156	1.0926	0.0005
CPO	18.3672	1.0204	0.0010
PCPO	5.0076	0.2334	**0.0003**

Table 22: Metrics of nine **Goal_{Robot}_8Ghosts** environments obtained from the final epoch.

Goal_Point_8Ghosts

Algorithm	$\bar{J}_r$	$\bar{M}_c$	$\bar{\rho}_c$
TRPO	26.0478	6.8329	0.0073
TRPO-Lagrangian	26.3260	**2.1498**	0.0034
TRPO-SL	16.6548	4.0515	0.0058
TRPO-USL	22.1795	5.8895	0.0059
TRPO-IPO	20.1808	4.1169	0.0050
TRPO-FAC	25.9489	2.5654	0.0036
CPO	**26.5064**	2.6248	**0.0034**
PCPO	25.9672	3.8589	0.0054

Goal_Swimmer_8Ghosts

Algorithm	$\bar{J}_r$	$\bar{M}_c$	$\bar{\rho}_c$
TRPO	**30.3401**	13.5808	0.0119
TRPO-Lagrangian	15.9952	**2.1046**	**0.0061**
TRPO-SL	7.8773	7.6875	0.0079
TRPO-USL	30.1229	8.9488	0.0105
TRPO-IPO	9.8646	10.0275	0.0091
TRPO-FAC	18.9950	4.4988	0.0069
CPO	26.6953	9.5202	0.0092
PCPO	26.2737	10.2204	0.0101

Goal_Ant_8Ghosts

Algorithm	$\bar{J}_r$	$\bar{M}_c$	$\bar{\rho}_c$
TRPO	59.6760	10.3785	0.0099
TRPO-Lagrangian	28.5846	**2.9654**	**0.0060**
TRPO-SL	30.7285	41.2262	0.0342
TRPO-USL	**61.2725**	8.9165	0.0097
TRPO-IPO	2.9659	8.0972	0.0064
TRPO-FAC	44.2423	5.6508	0.0074
CPO	56.3422	9.8690	0.0095
PCPO	58.4684	9.8173	0.0095

Goal_Walker_8Ghosts

Algorithm	$\bar{J}_r$	$\bar{M}_c$	$\bar{\rho}_c$
TRPO	**63.2017**	9.8771	0.0112
TRPO-Lagrangian	33.2534	**2.5072**	**0.0054**
TRPO-SL	37.8968	20.3758	0.0147
TRPO-USL	61.4547	9.6043	0.0105
TRPO-IPO	7.4640	9.1178	0.0080
TRPO-FAC	45.0094	4.9375	0.0071
CPO	60.1257	9.2117	0.0097
PCPO	43.8760	9.2932	0.0085

Goal_Humanoid_8Ghosts

Algorithm	$\bar{J}_r$	$\bar{M}_c$	$\bar{\rho}_c$
TRPO	11.1891	9.9692	0.0098
TRPO-Lagrangian	5.0070	**6.6812**	0.0076
TRPO-SL	8.8939	17.0632	0.0107
TRPO-USL	10.6905	9.6248	0.0095
TRPO-IPO	1.0404	8.4966	**0.0073**
TRPO-FAC	9.2134	10.0716	0.0084
CPO	10.0778	10.3074	0.0092
PCPO	**11.5003**	9.0205	0.0093

Goal_Hopper_8Ghosts

Algorithm	$\bar{J}_r$	$\bar{M}_c$	$\bar{\rho}_c$
TRPO	**31.6643**	8.1599	0.0100
TRPO-Lagrangian	14.1699	**4.4744**	**0.0070**
TRPO-SL	21.7761	12.4810	0.0122
TRPO-USL	31.2864	8.4550	0.0097
TRPO-IPO	5.4826	12.0015	0.0082
TRPO-FAC	28.8157	7.5453	0.0087
CPO	29.0408	7.5681	0.0086
PCPO	29.0858	8.0181	0.0090

Goal_Arm3_8Ghosts

Algorithm	$\bar{J}_r$	$\bar{M}_c$	$\bar{\rho}_c$
TRPO	94.6660	35.7460	0.0348
TRPO-Lagrangian	15.4898	7.5123	**0.0058**
TRPO-SL	18.1207	10.7580	0.0174
TRPO-USL	62.1624	14.0682	0.0223
TRPO-IPO	4.0235	10.5251	0.0160
TRPO-FAC	37.9750	**6.9701**	0.0073
CPO	114.8705	15.1904	0.0159
PCPO	**126.4001**	10.1913	0.0143

Goal_Arm6_8Ghosts

Algorithm	$\bar{J}_r$	$\bar{M}_c$	$\bar{\rho}_c$
TRPO	1.0157	49.0135	0.0466
TRPO-Lagrangian	0.5470	**8.4307**	0.0190
TRPO-SL	0.6078	20.5269	0.0356
TRPO-USL	0.9856	41.7054	0.0427
TRPO-IPO	0.7336	12.4453	0.0233
TRPO-FAC	0.7861	9.4493	0.0170
CPO	**9.9993**	22.5031	0.0234
PCPO	0.8845	15.9718	**0.0162**

Goal_Drone_8Ghosts

Algorithm	$\bar{J}_r$	$\bar{M}_c$	$\bar{\rho}_c$
TRPO	17.9484	1.7287	0.0011
TRPO-Lagrangian	18.9773	0.9218	0.0008
TRPO-SL	12.1413	**0.2500**	0.0004
TRPO-USL	10.7517	0.9741	0.0011
TRPO-IPO	11.5210	0.6817	0.0006
TRPO-FAC	**20.1014**	0.7630	0.0006
CPO	18.4723	1.2188	0.0008
PCPO	6.5276	0.3859	**0.0003**

Table 23: Metrics of nine **Push_{Robot}_8Hazards** environments obtained from the final epoch.

Push_Point_8Hazards

Algorithm	$\bar{J}_r$	$\bar{M}_c$	$\bar{\rho}_c$
TRPO	**11.3060**	7.2536	0.0084
TRPO-Lagrangian	4.1189	**1.8268**	**0.0037**
TRPO-SL	3.0553	6.6139	0.0058
TRPO-USL	9.1904	6.6179	0.0064
TRPO-IPO	1.3370	4.0476	0.0051
TRPO-FAC	6.0431	2.1250	0.0039
CPO	9.7522	5.6406	0.0066
PCPO	9.1434	6.5665	0.0066

Push_Swimmer_8Hazards

Algorithm	$\bar{J}_r$	$\bar{M}_c$	$\bar{\rho}_c$
TRPO	**86.1557**	11.9235	0.0102
TRPO-Lagrangian	52.0782	**4.5645**	0.0070
TRPO-SL	13.1869	7.7554	**0.0057**
TRPO-USL	64.0705	9.4963	0.0085
TRPO-IPO	6.3843	8.4329	0.0077
TRPO-FAC	48.2986	5.8675	0.0064
CPO	57.4370	6.9551	0.0072
PCPO	56.2598	6.1634	0.0076

Push_Ant_8Hazards

Algorithm	$\bar{J}_r$	$\bar{M}_c$	$\bar{\rho}_c$
TRPO	**13.4378**	9.4740	0.0091
TRPO-Lagrangian	1.1582	**1.5948**	**0.0043**
TRPO-SL	3.5622	47.7602	0.0217
TRPO-USL	11.2763	9.3930	0.0086
TRPO-IPO	1.1986	5.9120	0.0061
TRPO-FAC	2.5905	2.7927	0.0050
CPO	12.7081	7.5742	0.0082
PCPO	11.0161	8.7780	0.0087

Push_Walker_8Hazards

Algorithm	$\bar{J}_r$	$\bar{M}_c$	$\bar{\rho}_c$
TRPO	**5.0574**	10.8840	0.0089
TRPO-Lagrangian	1.5035	**2.4237**	**0.0040**
TRPO-SL	1.7263	17.5680	0.0082
TRPO-USL	2.8786	9.3900	0.0078
TRPO-IPO	0.7991	3.6377	0.0070
TRPO-FAC	1.5393	3.2465	0.0047
CPO	4.3412	7.8450	0.0075
PCPO	1.1548	9.2470	0.0075

Push_Humanoid_8Hazards

Algorithm	$\bar{J}_r$	$\bar{M}_c$	$\bar{\rho}_c$
TRPO	0.9545	10.6542	0.0096
TRPO-Lagrangian	0.7407	3.1758	**0.0062**
TRPO-SL	0.2992	9.0239	0.0092
TRPO-USL	0.8102	7.3410	0.0093
TRPO-IPO	0.8194	6.0952	0.0074
TRPO-FAC	0.9641	**3.0034**	0.0068
CPO	0.8147	8.6884	0.0080
PCPO	**1.0445**	8.1230	0.0084

Push_Hopper_8Hazards

Algorithm	$\bar{J}_r$	$\bar{M}_c$	$\bar{\rho}_c$
TRPO	**3.6134**	10.3693	0.0095
TRPO-Lagrangian	0.8384	**2.0782**	**0.0052**
TRPO-SL	1.5115	8.2643	0.0080
TRPO-USL	2.3949	11.2835	0.0088
TRPO-IPO	0.3718	7.4184	0.0083
TRPO-FAC	1.0928	3.8033	0.0069
CPO	2.3108	11.2012	0.0082
PCPO	0.9565	8.8373	0.0083

Push_Arm3_8Hazards

Algorithm	$\bar{J}_r$	$\bar{M}_c$	$\bar{\rho}_c$
TRPO	0.0438	37.7114	0.0414
TRPO-Lagrangian	-194.8455	**2.7071**	**0.0062**
TRPO-SL	**0.0906**	7.3980	0.0176
TRPO-USL	-42.2457	10.6065	0.0189
TRPO-IPO	-420.0890	25.0669	0.0224
TRPO-FAC	-114.8912	7.8944	0.0086
CPO	0.0249	11.3773	0.0128
PCPO	-30.9294	10.4467	0.0207

Push_Arm6_8Hazards

Algorithm	$\bar{J}_r$	$\bar{M}_c$	$\bar{\rho}_c$
TRPO	1.1128	15.9080	0.0190
TRPO-Lagrangian	0.9490	7.1961	0.0110
TRPO-SL	-220.2115	38.7175	0.0144
TRPO-USL	-0.6530	16.7103	0.0182
TRPO-IPO	1.1291	8.3642	0.0113
TRPO-FAC	1.0648	9.4750	0.0152
CPO	**1.1699**	**6.6375**	**0.0103**
PCPO	1.1459	10.0104	0.0112

Push_Drone_8Hazards

Algorithm	$\bar{J}_r$	$\bar{M}_c$	$\bar{\rho}_c$
TRPO	0.9332	0.3324	0.0002
TRPO-Lagrangian	1.0967	0.3197	0.0003
TRPO-SL	1.0154	0.0783	0.0001
TRPO-USL	0.9410	0.0996	0.0001
TRPO-IPO	1.0394	0.4229	0.0002
TRPO-FAC	1.0820	0.2380	0.0002
CPO	**1.1261**	0.2409	0.0003
PCPO	0.9844	**0.0049**	**0.0001**

Table 24: Metrics of nine **Chase_{Robot}_8Hazards** environments obtained from the final epoch.

Chase_Point_8Hazards

Algorithm	$\bar{J}_r$	$\bar{M}_c$	$\bar{\rho}_c$
TRPO	**1.3122**	3.5553	0.0068
TRPO-Lagrangian	1.0879	**2.8816**	**0.0046**
TRPO-SL	0.8385	5.6000	0.0058
TRPO-USL	1.1433	5.7574	0.0080
TRPO-IPO	0.7959	8.5632	0.0061
TRPO-FAC	1.0333	3.0887	0.0053
CPO	1.2897	5.0677	0.0063
PCPO	1.0035	7.9018	0.0084

Chase_Swimmer_8Hazards

Algorithm	$\bar{J}_r$	$\bar{M}_c$	$\bar{\rho}_c$
TRPO	1.2491	7.0269	0.0100
TRPO-Lagrangian	-0.2346	**4.8860**	**0.0058**
TRPO-SL	0.0518	9.2681	0.0071
TRPO-USL	1.2227	9.2911	0.0103
TRPO-IPO	-1.0848	10.5546	0.0080
TRPO-FAC	0.6411	9.1446	0.0078
CPO	**1.2540**	8.1671	0.0082
PCPO	1.2152	8.2717	0.0090

Chase_Ant_8Hazards

Algorithm	$\bar{J}_r$	$\bar{M}_c$	$\bar{\rho}_c$
TRPO	1.3504	6.1101	0.0106
TRPO-Lagrangian	-0.3563	**2.5016**	**0.0040**
TRPO-SL	0.7921	16.9846	0.0222
TRPO-USL	1.3841	8.0640	0.0096
TRPO-IPO	-0.9314	2.5529	0.0048
TRPO-FAC	-0.0258	3.5439	0.0048
CPO	**1.4104**	5.7863	0.0087
PCPO	1.3122	6.9139	0.0097

Chase_Walker_8Hazards

Algorithm	$\bar{J}_r$	$\bar{M}_c$	$\bar{\rho}_c$
TRPO	0.4890	7.6845	0.0088
TRPO-Lagrangian	-0.0922	2.5167	0.0045
TRPO-SL	-0.2116	10.7167	0.0094
TRPO-USL	0.4639	7.7035	0.0082
TRPO-IPO	-0.8223	**2.3954**	**0.0038**
TRPO-FAC	-0.0368	2.7105	0.0047
CPO	**0.7406**	10.4993	0.0086
PCPO	0.6347	8.8652	0.0080

Chase_Humanoid_8Hazards

Algorithm	$\bar{J}_r$	$\bar{M}_c$	$\bar{\rho}_c$
TRPO	**0.2330**	12.1455	0.0152
TRPO-Lagrangian	-0.6855	**3.4234**	**0.0047**
TRPO-SL	-0.2271	11.8001	0.0121
TRPO-USL	-0.1503	18.6011	0.0149
TRPO-IPO	-0.8074	6.4163	0.0054
TRPO-FAC	-0.5826	3.6663	0.0050
CPO	-0.3322	12.1665	0.0109
PCPO	-0.0971	10.3441	0.0113

Chase_Hopper_8Hazards

Algorithm	$\bar{J}_r$	$\bar{M}_c$	$\bar{\rho}_c$
TRPO	**0.6099**	12.1675	0.0134
TRPO-Lagrangian	-0.3641	**3.2170**	**0.0039**
TRPO-SL	0.4957	5.4355	0.0089
TRPO-USL	0.4819	11.0919	0.0123
TRPO-IPO	-0.7766	6.1236	0.0061
TRPO-FAC	-0.3651	3.7391	0.0055
CPO	0.4829	6.7117	0.0083
PCPO	-0.1457	7.4290	0.0068

Chase_Arm3_8Hazards

Algorithm	$\bar{J}_r$	$\bar{M}_c$	$\bar{\rho}_c$
TRPO	0.7772	20.6230	0.0312
TRPO-Lagrangian	-0.2739	5.1692	**0.0079**
TRPO-SL	0.0007	4.2869	0.0142
TRPO-USL	0.7825	14.1736	0.0284
TRPO-IPO	-0.4137	10.6685	0.0223
TRPO-FAC	0.3648	**3.3449**	0.0127
CPO	**0.8051**	17.4917	0.0252
PCPO	0.7355	25.8202	0.0291

Chase_Arm6_8Hazards

Algorithm	$\bar{J}_r$	$\bar{M}_c$	$\bar{\rho}_c$
TRPO	-0.3969	60.5704	0.0598
TRPO-Lagrangian	-0.4860	**2.4602**	**0.0075**
TRPO-SL	-0.5420	12.1256	0.0237
TRPO-USL	-0.5734	53.4455	0.0575
TRPO-IPO	**-0.2855**	11.6769	0.0085
TRPO-FAC	-0.3083	13.2429	0.0263
CPO	-0.3278	16.9609	0.0247
PCPO	-0.2883	45.6164	0.0463

Chase_Drone_8Hazards

Algorithm	$\bar{J}_r$	$\bar{M}_c$	$\bar{\rho}_c$
TRPO	1.0351	0.6939	0.0008
TRPO-Lagrangian	0.8211	1.3456	0.0008
TRPO-SL	-1.3055	0.2603	**0.0002**
TRPO-USL	0.7461	1.2159	0.0006
TRPO-IPO	0.2518	0.5786	0.0005
TRPO-FAC	**1.1192**	**0.2374**	0.0006
CPO	0.7682	0.9075	0.0006
PCPO	0.6172	0.6374	0.0012

Table 25: Metrics of nine **Defense__{Robot}__8Hazards** environments obtained from the final epoch.

Defense__Point__8Hazards

Algorithm	$\bar{J}_r$	$\bar{M}_c$	$\bar{\rho}_c$
TRPO	**71.7851**	37.5050	0.0308
TRPO-Lagrangian	-12.2159	1.1776	0.0026
TRPO-SL	-89.8828	3.1691	0.0070
TRPO-USL	-109.7828	9.9285	0.0086
TRPO-IPO	-330.4252	**0.7309**	0.0035
TRPO-FAC	-269.0397	0.7334	**0.0015**
CPO	36.7643	7.1534	0.0071
PCPO	19.0943	1.9388	0.0048

Defense__Swimmer__8Hazards

Algorithm	$\bar{J}_r$	$\bar{M}_c$	$\bar{\rho}_c$
TRPO	119.9896	44.5965	0.0405
TRPO-Lagrangian	-85.0177	**0.2487**	**0.0031**
TRPO-SL	-41.8928	1.3295	0.0118
TRPO-USL	**139.8915**	13.5482	0.0150
TRPO-IPO	-233.1962	7.6313	0.0070
TRPO-FAC	-91.7454	0.8809	0.0032
CPO	34.3226	2.7346	0.0072
PCPO	91.1387	5.1068	0.0084

Defense__Ant__8Hazards

Algorithm	$\bar{J}_r$	$\bar{M}_c$	$\bar{\rho}_c$
TRPO	**65.9815**	46.1871	0.0214
TRPO-Lagrangian	-190.9671	1.5799	**0.0040**
TRPO-SL	-15.0035	14.7914	0.0143
TRPO-USL	-9.1186	25.8625	0.0126
TRPO-IPO	-205.8713	6.0119	0.0044
TRPO-FAC	-204.4595	**1.4105**	0.0041
CPO	-22.6369	17.9356	0.0132
PCPO	-42.0119	17.1633	0.0120

Defense__Walker__8Hazards

Algorithm	$\bar{J}_r$	$\bar{M}_c$	$\bar{\rho}_c$
TRPO	**63.0381**	52.1661	0.0326
TRPO-Lagrangian	-221.9464	**0.8080**	**0.0032**
TRPO-SL	-28.2392	21.2179	0.0142
TRPO-USL	19.2097	23.4844	0.0182
TRPO-IPO	-213.4079	2.7606	0.0045
TRPO-FAC	-183.6202	1.6905	0.0035
CPO	32.0705	14.7761	0.0151
PCPO	43.8441	17.0562	0.0161

Defense__Humanoid__8Hazards

Algorithm	$\bar{J}_r$	$\bar{M}_c$	$\bar{\rho}_c$
TRPO	-279.6928	4.3248	0.0042
TRPO-Lagrangian	-287.5846	3.0248	0.0035
TRPO-SL	-325.6846	2.0650	0.0039
TRPO-USL	-318.2901	3.5935	0.0043
TRPO-IPO	-281.2530	4.3968	0.0038
TRPO-FAC	-271.4645	**2.0044**	**0.0034**
CPO	**-246.6409**	5.8980	0.0049
PCPO	-317.0349	2.9953	0.0040

Defense__Hopper__8Hazards

Algorithm	$\bar{J}_r$	$\bar{M}_c$	$\bar{\rho}_c$
TRPO	-79.4386	26.9427	0.0202
TRPO-Lagrangian	-304.2345	1.1963	**0.0029**
TRPO-SL	-207.0506	8.9198	0.0138
TRPO-USL	**57.7316**	28.5037	0.0234
TRPO-IPO	-248.0784	6.6735	0.0046
TRPO-FAC	-233.1694	**0.7496**	0.0038
CPO	-271.5419	8.3413	0.0077
PCPO	-279.4999	7.2803	0.0077

Defense__Arm3__8Hazards

Algorithm	$\bar{J}_r$	$\bar{M}_c$	$\bar{\rho}_c$
TRPO	169.5352	22.0750	0.0301
TRPO-Lagrangian	151.7291	**0.7971**	**0.0056**
TRPO-SL	112.3637	1.1085	0.0160
TRPO-USL	164.4992	5.3212	0.0163
TRPO-IPO	94.1636	9.1085	0.0171
TRPO-FAC	**180.9871**	1.7731	0.0064
CPO	167.4984	16.4595	0.0162
PCPO	160.2841	22.2282	0.0189

Defense__Arm6__8Hazards

Algorithm	$\bar{J}_r$	$\bar{M}_c$	$\bar{\rho}_c$
TRPO	**183.9203**	56.5334	0.0548
TRPO-Lagrangian	169.9900	**1.0108**	**0.0045**
TRPO-SL	171.8430	13.3277	0.0229
TRPO-USL	183.7060	52.3346	0.0528
TRPO-IPO	127.3447	3.8719	0.0051
TRPO-FAC	175.8257	2.3101	0.0109
CPO	174.7701	22.8158	0.0346
PCPO	174.4207	30.1276	0.0264

Defense__Drone__8Hazards

Algorithm	$\bar{J}_r$	$\bar{M}_c$	$\bar{\rho}_c$
TRPO	-241.5720	0.0771	0.0002
TRPO-Lagrangian	-245.7311	0.2276	0.0002
TRPO-SL	-371.7727	**0.0000**	**0.0001**
TRPO-USL	-336.7727	0.2161	0.0001
TRPO-IPO	-275.5550	0.2600	0.0002
TRPO-FAC	-215.4844	0.0691	0.0001
CPO	**-212.1858**	0.0236	0.0002
PCPO	-219.4308	0.3358	0.0003

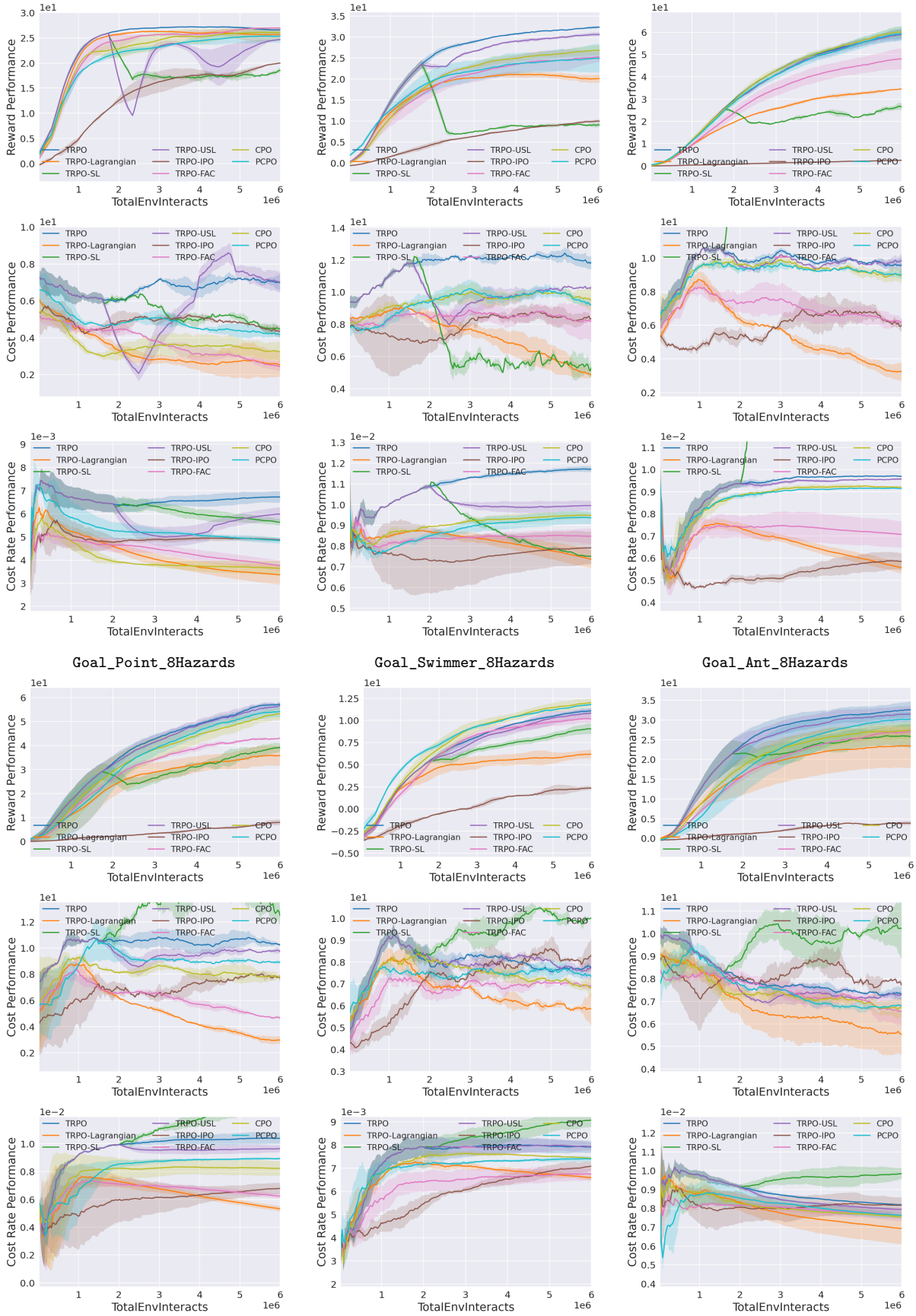

Goal_Point_8Hazards

Goal_Swimmer_8Hazards

Goal_Ant_8Hazards

Goal_Walker_8Hazards

Goal_Humanoid_8Hazards

Goal_Hopper_8Hazards

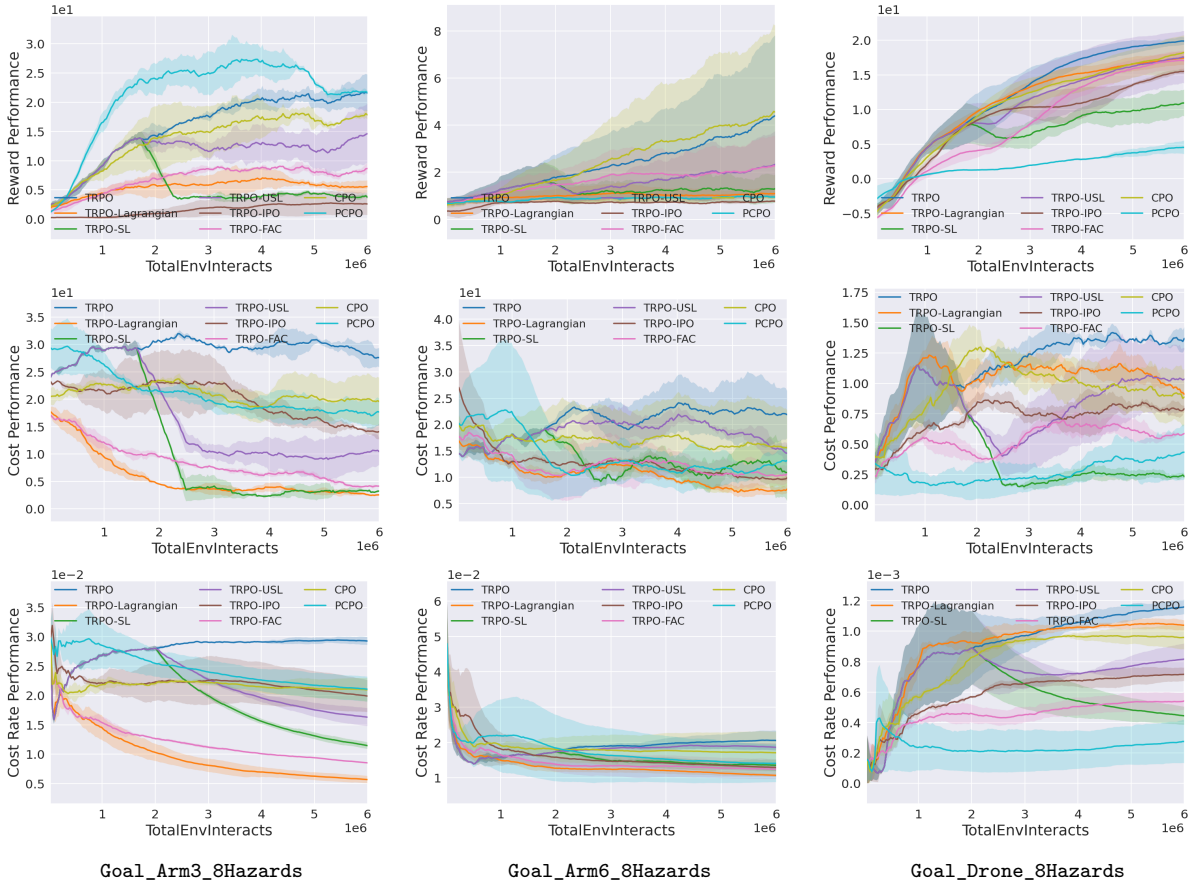

Figure 13: `Goal_{Robot}_8Hazards`

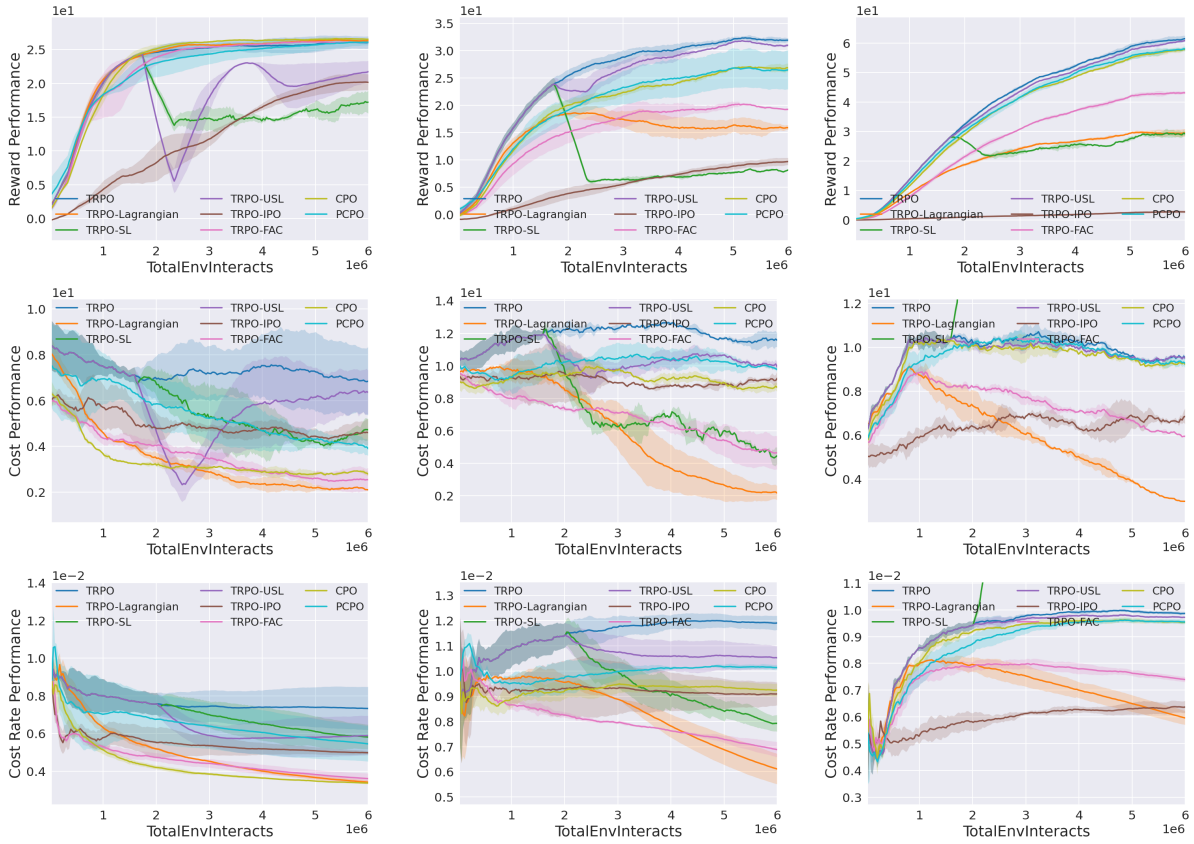

Goal_Point_8Ghosts Goal_Swimmer_8Ghosts Goal_Ant_8Ghosts

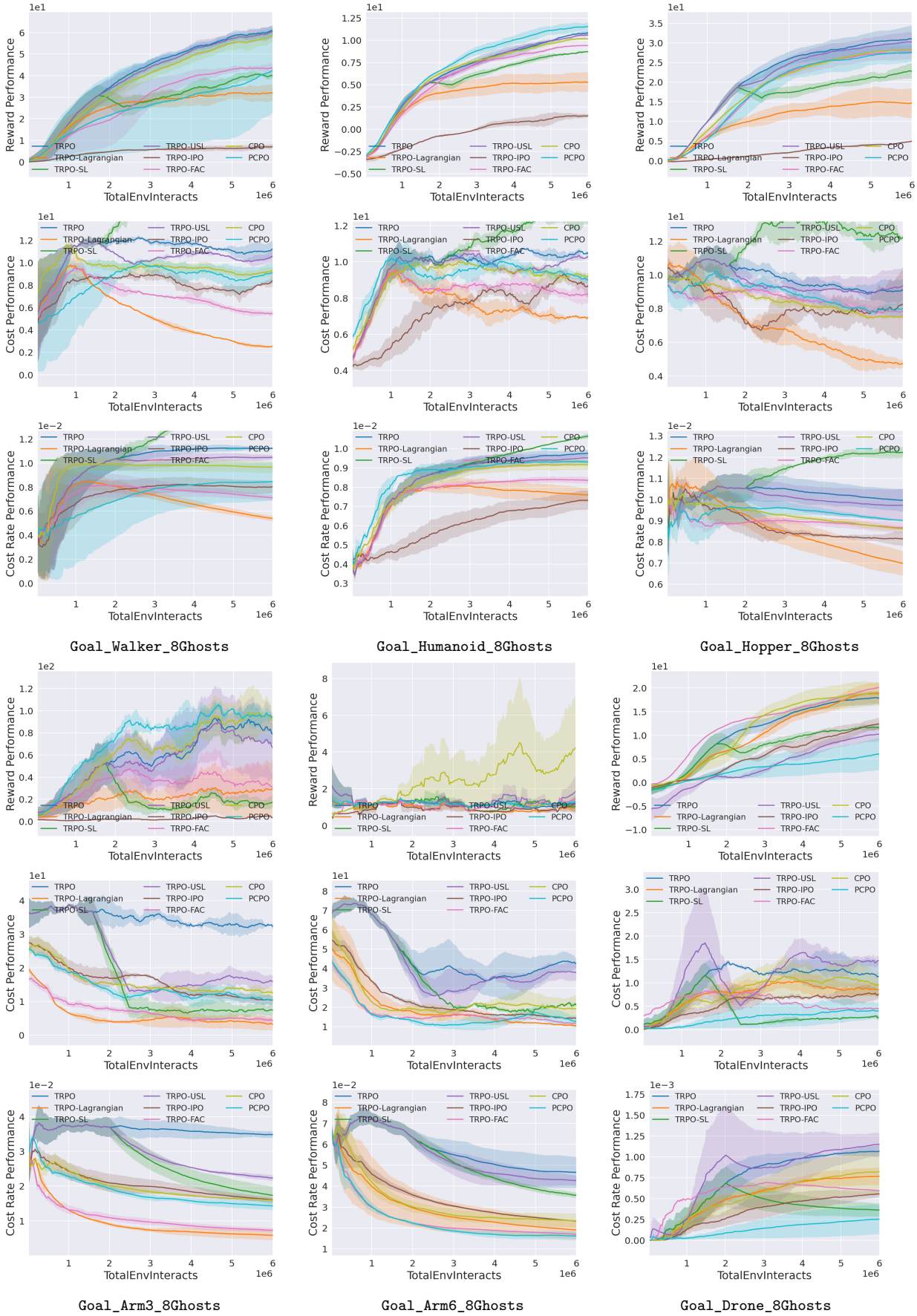

Figure 14: `Goal_{Robot}_8Ghosts`

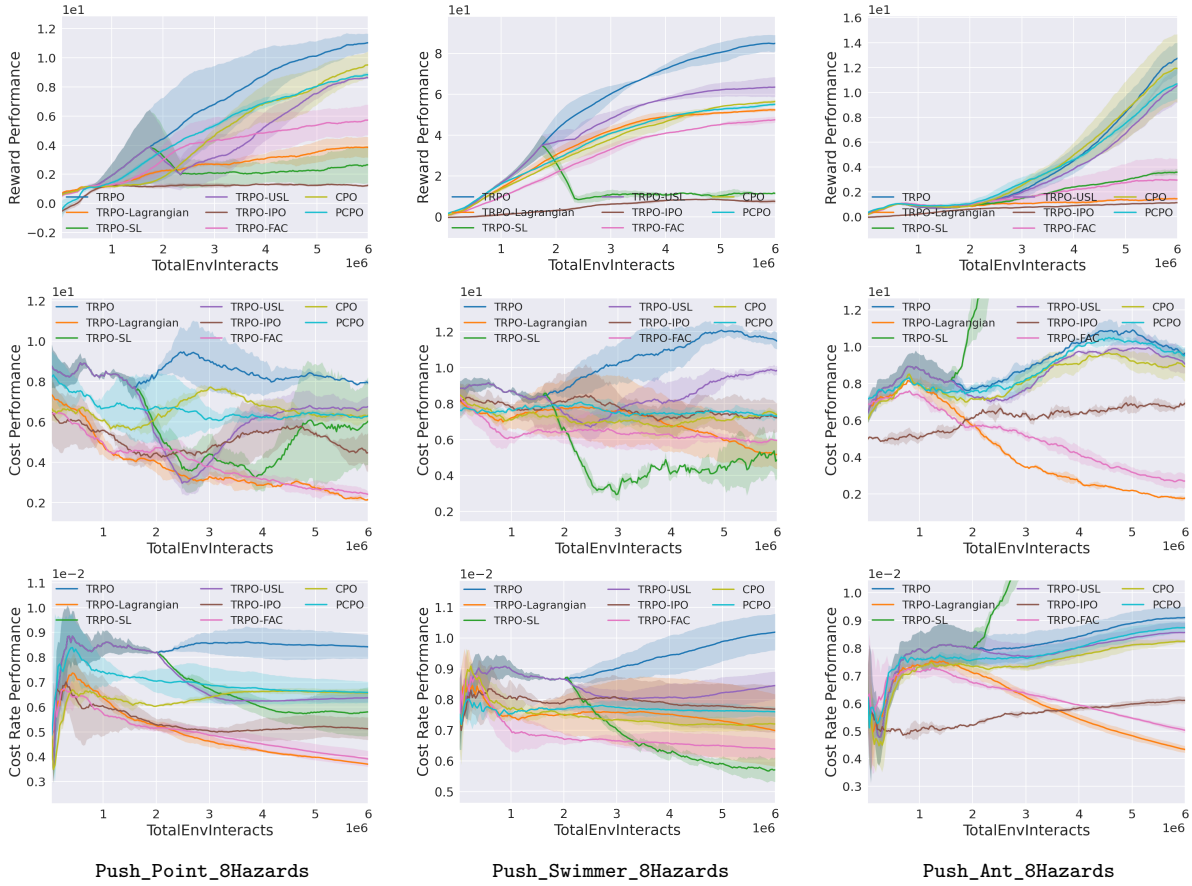

Push_Point_8Hazards Push_Swimmer_8Hazards Push_Ant_8Hazards

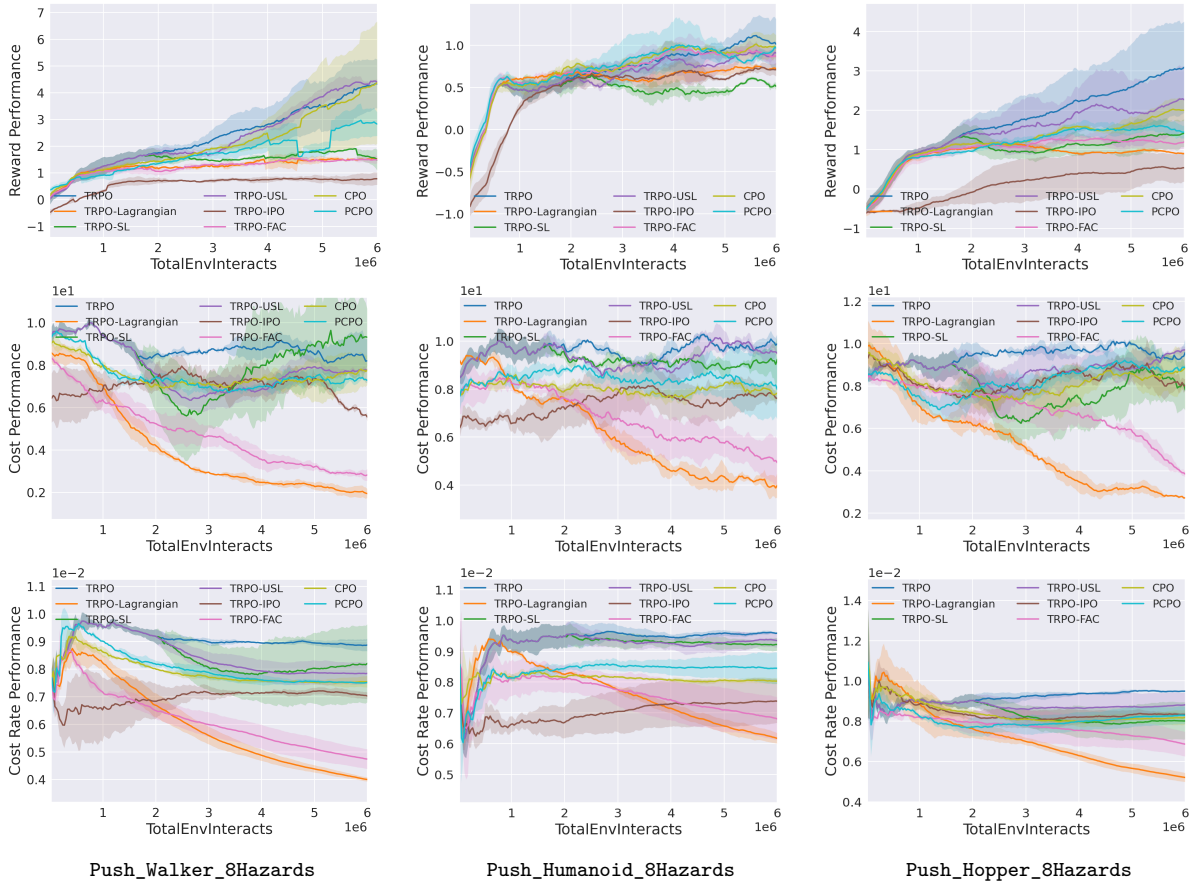

Push_Walker_8Hazards Push_Humanoid_8Hazards Push_Hopper_8Hazards

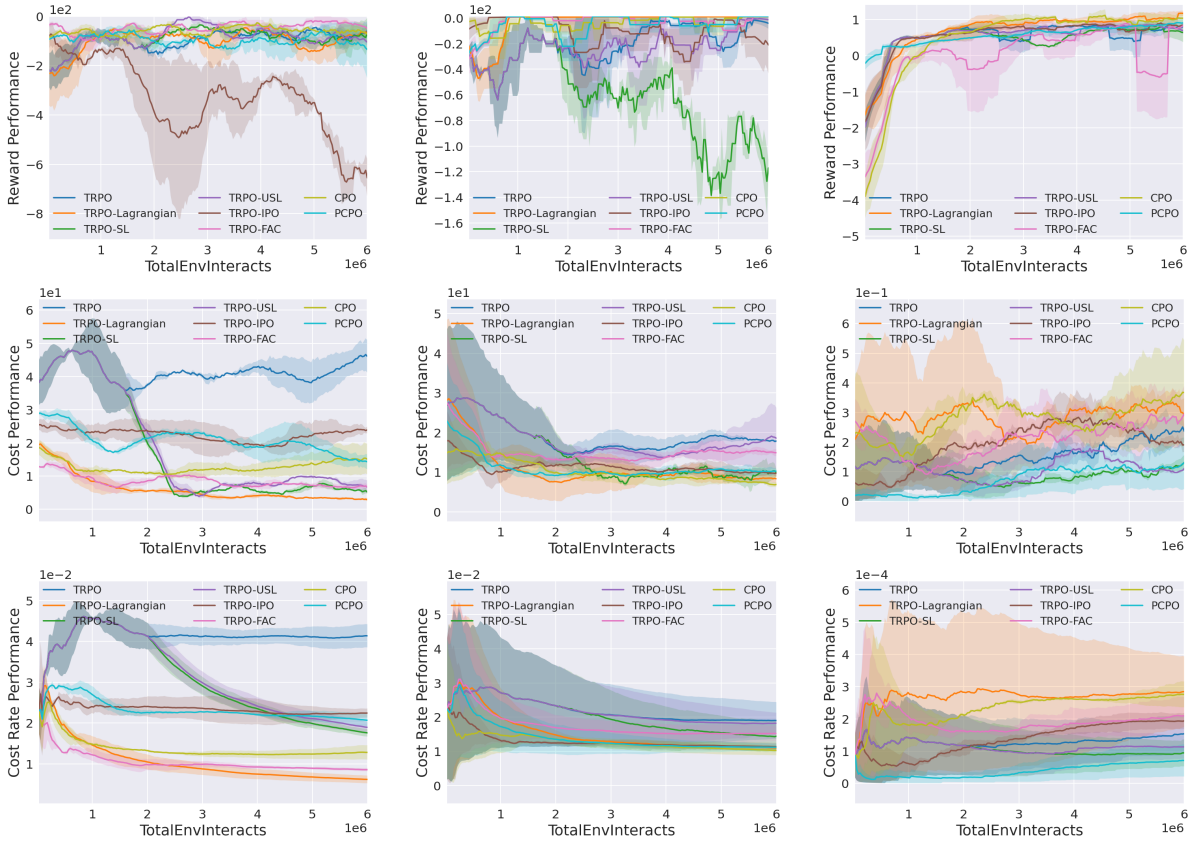

Push_Arm3_8Hazards Push_Arm6_8Hazards Push_Drone_8Hazards

Figure 15: Push_{Robot}_8Hazards

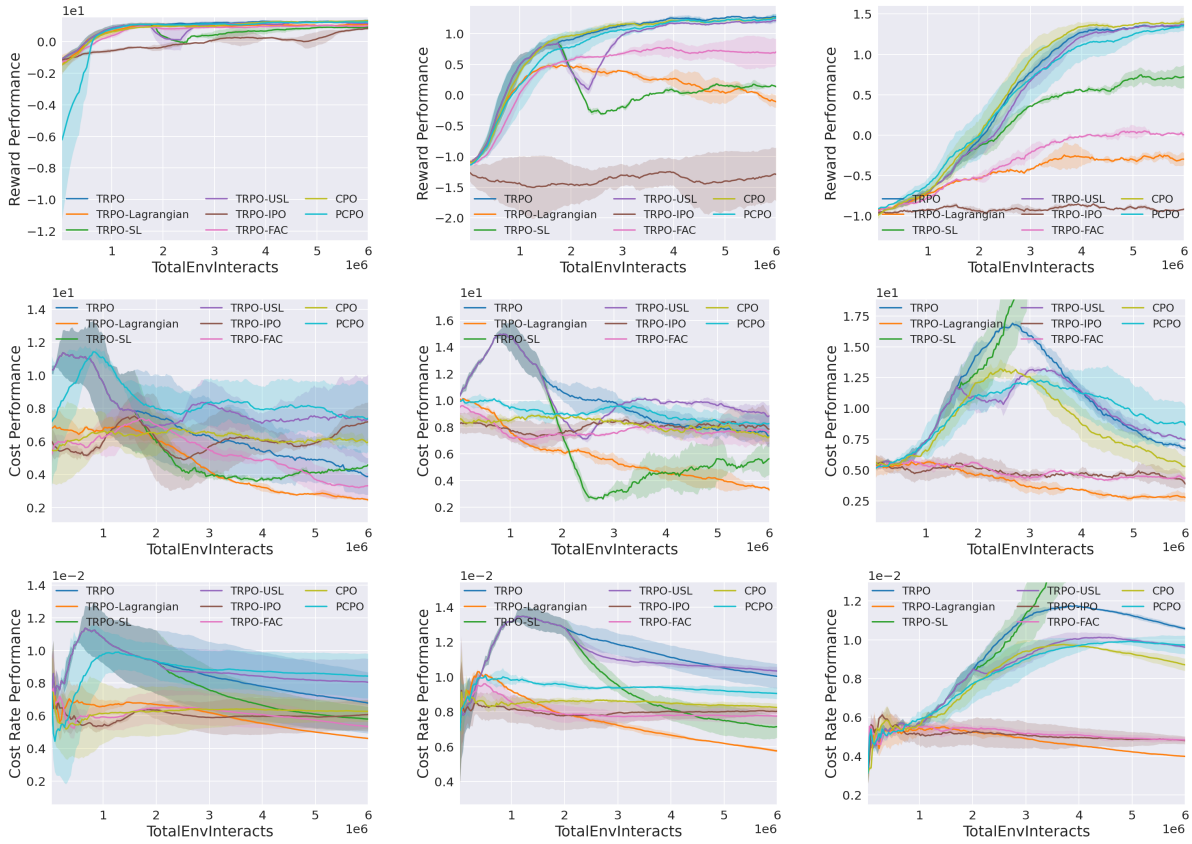

Chase_Point_8Hazards Chase_Swimmer_8Hazards Chase_Ant_8Hazards

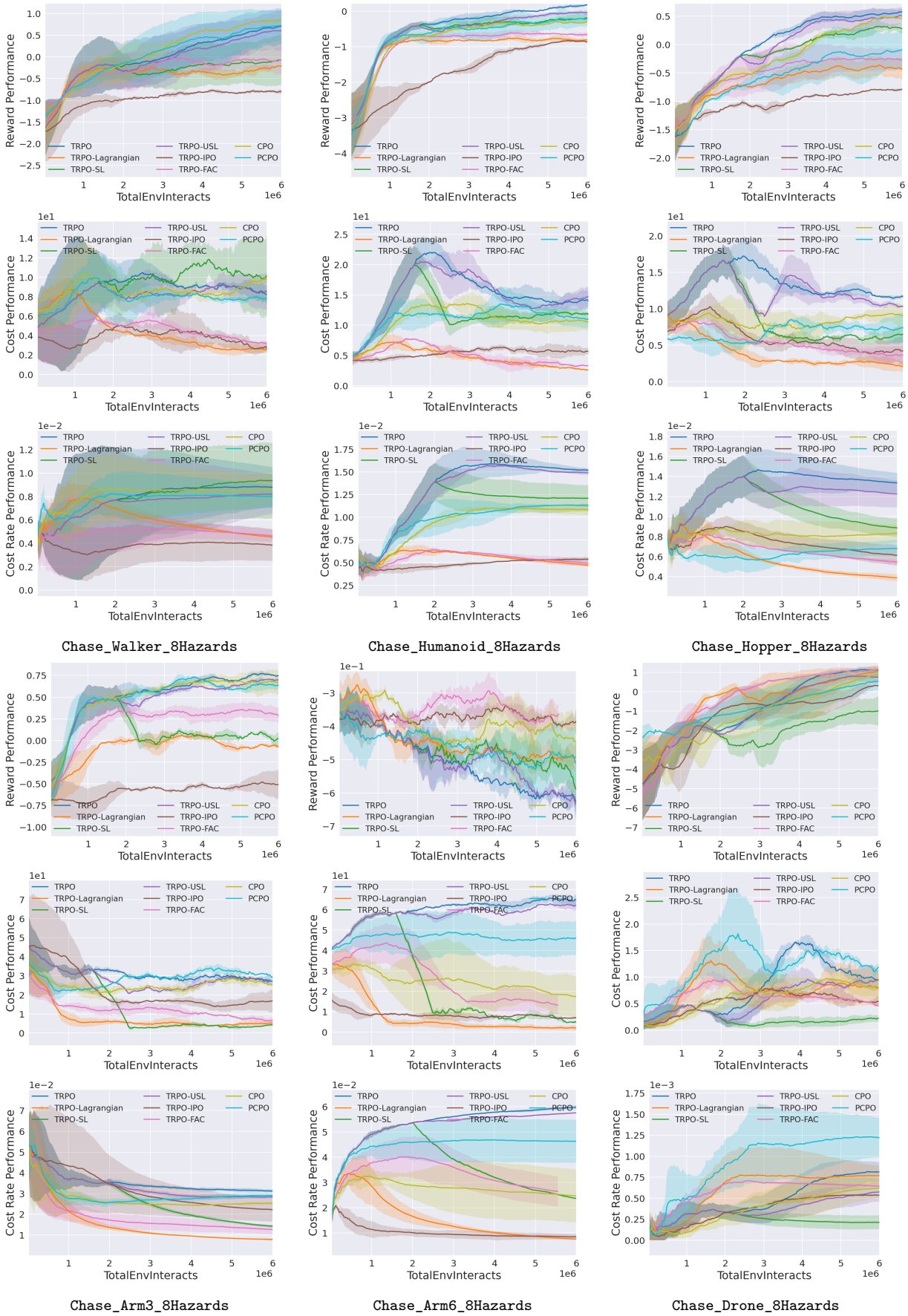

Figure 16: `Chase_{Robot}_8Hazards`

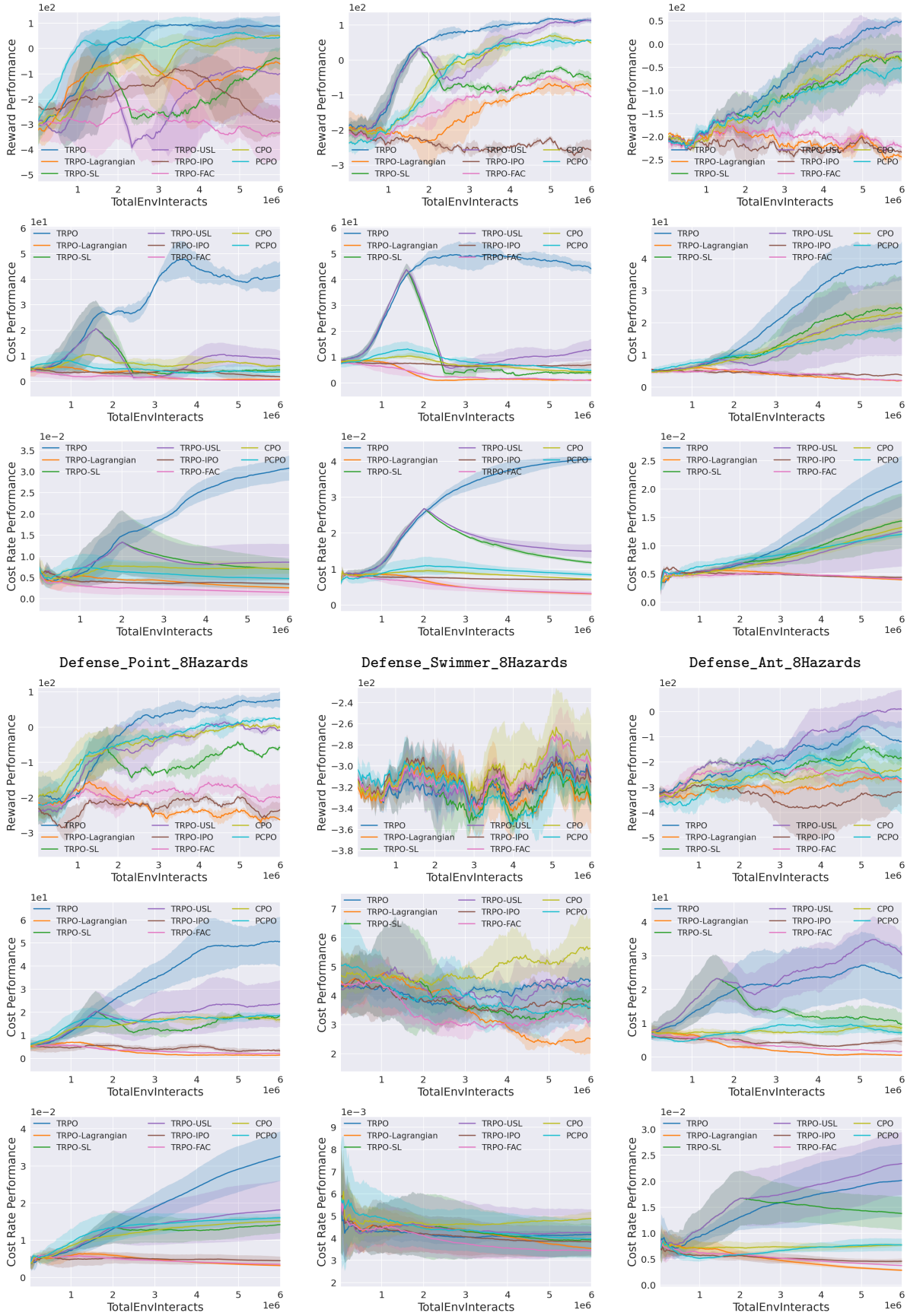

Defense_Point_8Hazards

Defense_Swimmer_8Hazards

Defense_Ant_8Hazards

Defense_Walker_8Hazards

Defense_Humanoid_8Hazards

Defense_Hopper_8Hazards

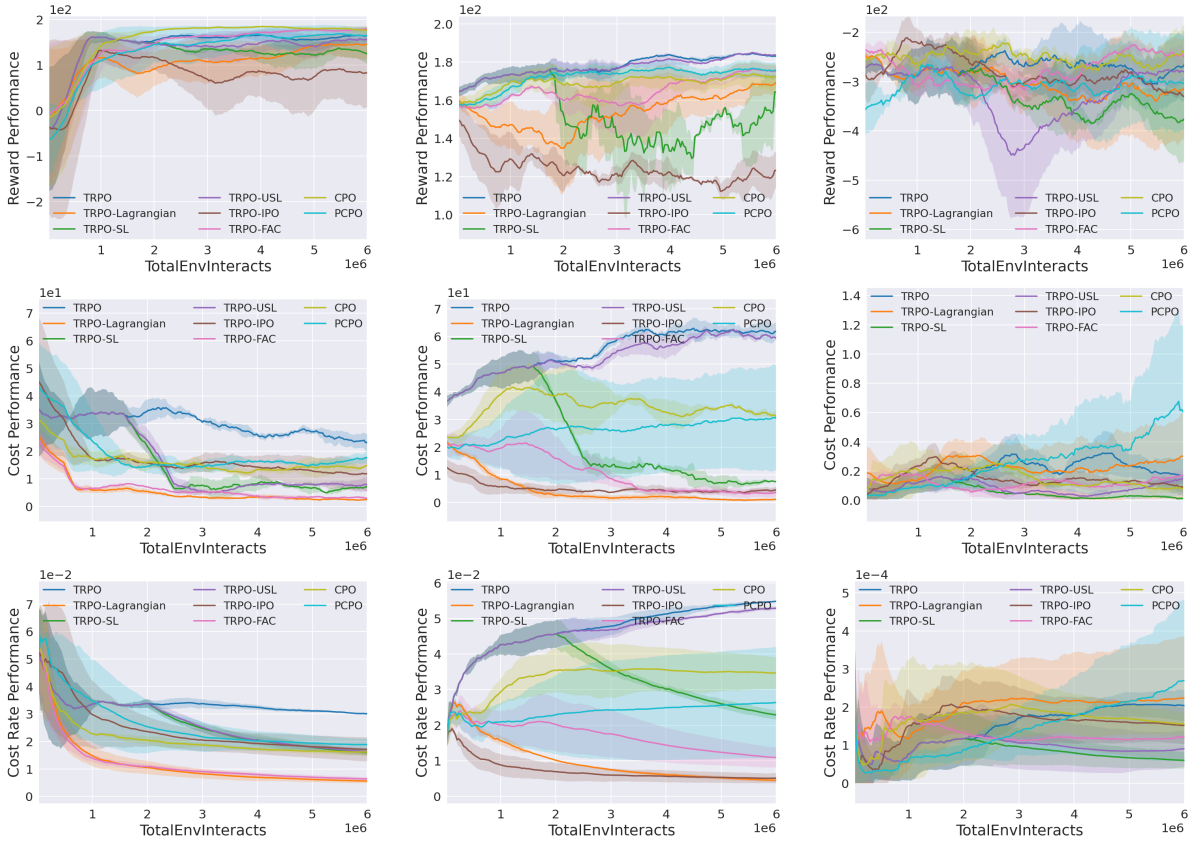

`Defense_Arm3_8Hazards` `Defense_Arm6_8Hazards` `Defense_Drone_8Hazards`

Figure 17: `Defense_{Robot}_8Hazards`